NOVEL HAEMODYNAMIC STRUCTURES IN THE HUMAN GLOMERULUS

Neal CR[1], Arkill KP[2], Bell JS[3], Betteridge KB[4], Bates DO[2], Winlove CP[5], Salmon AHJ[6], Harper SJ[1]

[1]Bristol Renal, Dorothy Hodgkin Building, University of Bristol, BS1 3NY, UK,
[2]Division of Cancer and Stem Cells, School of Medicine, University of Nottingham, Queen's Medical Centre, Nottingham NG7 2UH, UK
[3]Cardiff Centre for Vision Science, Cardiff University, Cardiff, CF24 4HQ
[4]Nikon Imaging Centre, Guys Campus, Kings College London, SE1 1UL
[5]School of Physics, University of Exeter, Stocker Road, Exeter, EX4 4QL, UK
[6]Waitemata District Health Board, Auckland, New Zealand

Running title: Novel Human Glomerular Vasculature

Keywords: glomerular microcirculation, haemodynamics, mesangial collagen, vascular chambers, conduit vessels

CRN - Kidney perfusions, resin tissue processing, serial sectioning, resin section reconstruction and 3D model construction, all measurements, plotting and statistics. Preparation for confocal and multiphoton microscopy. Electron microscopy, model and data interpretation, vascular chamber and conduit discovery, writing manuscript.
KPA - Reconstruction imaging, software assistance, multi-photon microscopy, manuscript
JSB - Multiphoton microscopy and software, manuscript
KBB - Confocal microscopy and software, manuscript
AHJS, CPW, DOB, SJH – interpretation, grant support, manuscript

Corresponding Author:
Chris Neal. Bristol Renal, Dorothy Hodgkin Building, University of Bristol, BS1 3NY, UK. +44 7599 169552. Chris.Neal@bristol.ac.uk

Abstract

To investigate human glomerular structure under conditions of physiological perfusion we have analysed fresh and perfusion fixed normal human glomeruli at physiological hydrostatic and oncotic pressures using serial resin section reconstruction, confocal, multiphoton and electron microscope imaging.

Afferent and efferent arterioles (21.5±1.2µm and 15.9±1.2µm diameter), recognised from vascular origins, lead into previously undescribed wider regions (43.2±2.8 µm and 38.4±4.9 µm diameter) we have termed vascular chambers (VCs) embedded in the mesangium of the vascular pole. Afferent VC(AVC) volume was 1.6 fold greater than Efferent VC(EVC) volume. From the AVC long non-branching high capacity conduit vessels (n=7) (Con; 15.9±0.7µm diameter) led to the glomerular edge where branching was more frequent. Conduit vessels have fewer podocytes than filtration capillaries. VCs were confirmed in fixed and unfixed specimens with a layer of banded collagen identified in AVC walls by multiphoton and electron microscopy. Thirteen highly branched efferent first order vessels (E1;9.9±0.4µm diam.) converge on the EVC draining into the efferent arteriole (15.9±1.2µm diam.). Banded collagen was scarce around EVC.

This previously undescribed branching topology does not conform to the branching of minimum energy expenditure (Murray's law), suggesting even distribution of pressure/flow to the filtration capillaries is more important than maintaining the minimum work required for blood flow. We propose that AVCs act as plenum manifolds possibly aided by vortical flow in distributing and balancing blood flow/pressure to conduit vessels supplying glomerular lobules. These major adaptations to glomerular capillary structure could regulate haemodynamic pressure and flow in human glomerular capillaries.

Introduction

The control of glomerular blood flow is crucial for maintaining efficient ultrafiltration across the glomerular filtration barrier (GFB). Glomerular disease is characterised by molecular and physiological perturbations and altered glomerular haemodynamics (intraglomerular pressure and hyper-perfusion), however, most of the models of glomerular haemodynamics in humans are based on experimental animals with small glomeruli. A few studies have attempted to reconstruct the human glomerular vascular network; a wax model of a human neonate glomerulus was reconstructed by Johnston in 1899 (21) and in 1956 plastic glomerular vessels were reconstructed from wax moulded outlines (6). These and later casting techniques render impressions of the glomerular surface capillaries with deeper vessels remaining largely hidden.

More recent computational methods have revealed nodes and branching in rat and human glomerular vasculature (33, 34, 47, 48, 53). The human reconstructions were performed on 5µm sections and/or on immersion fixed sources or only on small glomerular regions and the few studies of the vascular pole of the human glomerulus have used biopsy or cadaver recovered material (33, 56). To date, only one reconstructive study has been published using perfusion-fixation of a human transplant kidney but at elevated hydrostatic pressure (140mm Hg) where the authors chose a stereological approach for vessel analysis rather than reconstruction (4).

Glomerular capillaries operate at relatively high pressure in life which in turn sets urinary driving pressure in the Bowman's capsule and tubules producing tubular flow. For instance, the human glomerular capillary hydrostatic pressure of 60 to 65 mmHg at the afferent end (43) falls only 2-3mmHg to the efferent end. Countering this filtration pressure is an afferent plasma colloid osmotic pressure of 25mmHg rising to 32mmHg at the efferent end (1). As a result of filtration, urinary space hydrostatic pressure is 20-25mmHg (61) pressurizing the proximal convoluted tubule producing flow through to the collecting duct and the renal hilus. Thus, the function and structure of the whole nephron relies upon the glomerular perfusion of an oncotically appropriate fluid at the correct hydrostatic pressure to raise the right physiological pressures and flows in the tubules. In biopsy/necropsy kidney specimens the absence of pressure during immersion fixation results in the collapse of both the glomeruli and tubules. Fixing at the correct physiological pressures (oncotic and hydrostatic) is therefore essential in investigating the true 'functionally inflated' architecture of the glomerulus.

We have previously shown that 3D ultrastructural reconstruction of animal and human glomeruli fixed under hydrostatic and oncotic physiological conditions allow the detailed analysis of the GFB and the identification of novel structural features such as the subpodocyte space (SPS)(39) One unexpected feature of light microscopic sections from these resin embedded human glomeruli was the frequency of wide vessel regions at the vascular pole when compared with rodent vascular poles implying different vascular structure. No mention of any such difference could be found in any recent study of human glomerular structure.

The haemodynamic requirements of rat and human glomeruli could shed light on any differing evolved morphologies. For instance, if glomerular volume is assumed to estimate perfused glomerular volume, this parameter does not scale in size with the increase in afferent arteriolar conductivity between rodents and humans. The human afferent arteriole has a conductivity 13 fold greater than that of the mouse (14000μm^4 vs 1100μm^4) but supplies a 23 fold larger glomerular volume [see Footnote 1]. Similarly, it is 3 times as conductive as that of the rat (4600μm^4), while supplying a 5 fold larger glomerular volume. If human glomerular morphology was simply scaled up from a small rodent pattern, then afferent arterioles should be closer to 26µm in diameter instead of 21µm.

This study therefore aimed to investigate these novel wide vascular regions of human glomeruli. How big were these regions? What was the wall structure and dimensions and were there any other associated features? Did the region constitute a wider region at the base of the afferent arteriole or a region of a thin walled capillary? Could these structural differences be involved in compensating for a high glomerular volume relative to the vascular input in human glomeruli? To address such questions, human kidneys were perfuse fixed (at physiological hydrostatic and oncotic pressures) and processed in such a way to reduce any accompanying tissue volume changes. Glomerular vasculature was observed and reconstructions made from fresh or fixed human kidney cortex using conventional light microscopy, confocal microscopy, multiphoton microscopy and transmission electron microscopy.

Methods

Fixation techniques

Human kidney tissue was sourced (with full ethical approval and consent of next of kin) from transplant kidneys (n=9) unused for technical reasons (eg poor major vessel condition, damage at retrieval, tumour in the contralateral kidney). The transport solution perfused through the kidney was Soltran (Potassium Citrate 0.86% w/v, Sodium Citrate 0.82% w/v, Mannitol 3.38% w/v, Magnesium Sulphate 1.0% w/v; Baxter Healthcare, UK). Approximately 2-3 litres of the solution was perfused through the kidney (200ml/minute, 120-140mmHg, 4°C) and then stored on ice. All other chemicals were sourced from Sigma-Aldrich, UK.

Kidneys were transported in ice-cold flush media. Centimetre diameter fresh cortical tissue was sampled from one pole for confocal and multiphoton microscopy and stored in chilled (4ºC) HEPES buffered Ringers solution. Smaller 1mm diameter tissue pieces were taken from the cut surface and fixed in 2.5% glutaraldehyde in HEPES buffer to serve as immersion fixed samples for TEM. At 4-10ºC kidneys were debrided of excess fat preserving the hilar components (renal artery, vein and ureter) and the sampled polar area of the kidney was clamped off with a large locking forceps. The renal artery was cannulated and the renal vein was cleared of any debris to allow outflow of perfusion fluid.

To offset any hyperfiltration and hyperperfusion during fixation normal hydrostatic and oncotic pressures were re-established by perfusing with an oncotically balanced (25mmHg oncotic pressure) flush solution (50ml, 20ºC). Colloid osmotic pressures were measured using a modified Hanson osmometer. The flush solution temperature was kept low to minimise autolytic/proteolytic activity. The hydrostatic pressure in the renal artery was set at 100mmHg (similar to human mean arterial pressure). After the flush bolus, 400ml of fixative was perfused through the kidney at the same pressures and temperature. Flush solution concentration was (mM); NaCl(132), KCl (4.6), $MgSO_4$ (1.3), $CaCl_2$ (2), HEPES (5), $NaHCO_3$ (25), D-glucose (5.5), 6.5% (w/v) Ficoll 400. Fixative was the same as the flush solution but with 1.25% (w/v) glutaraldehyde. The glycocalyx stain 0.5% lanthanum nitrate and 0.5% dysprosium chloride was incorporated into the solutions in 2 kidneys.

1mm diameter samples of perfusion fixed kidney were taken from a medial sub-capsular position and together with subcapsular immersion fixed samples were post-fixed in osmium tetroxide, dehydrated with ethanol and processed into Araldite resin using standard procedures.

To promote consistency in structural comparisons, measurement and observations were limited on the glomeruli of the outer (subcapsular) cortex of kidneys in a medial location half way between the poles (unless otherwise stated).

Reconstruction of vascular poles from perfusion fixed kidneys

Seven areas of resin embedded kidneys (n=4) which contained a high density of glomeruli were identified in Toluidine Blue stained sections. These areas were serially sectioned on a Reichert Ultracut microtome at 1µm thickness (2,095 sections approximately 300 sections per area). From these serial section runs, 3 or 4 fully sectioned glomeruli from each kidney were selected that clearly showed a vascular pole. The afferent arterioles of each of the 14 glomeruli were identified by tracing to a larger artery and/or the efferent arteriole traced to a peritubular position.

Digital micrographs (1,834) of serial sections of glomeruli (n=14) were made using a x40 objective on a Nikon E400 microscope. Digital images were repositioned, aligned, calibrated and measured using Image J software (NIH opensource ImageJ 1.46r & 1.47o) and compiled into image stacks. Topological maps were made of the route and diameter of the blood vessels coursing through the afferent and efferent parts of the vascular pole.

Resin section thickness calibration and glomerular diameter

Measurement and reconstruction in the sectioning direction is reliant upon the precision of the ultramicrotome mechanism controlling section thickness. To test the accuracy of the ultramicrotome, glomeruli were assumed to be spherical and of similar diameter in all directions. Glomerular diameter was measured in the sectioning direction (z) as well as in the section plane (x,y). An ellipse was fitted over the largest glomerular profile of a section image (x,y) and maximum and minimum diameters measured from this, the results were pooled (194.4±5.1µm n=28). In the image stacks of a glomerulus the first and last sections to contain the edge of glomerular blood vessels were found and the number of intervening sections counted (202.4±5.0 n=14). Assuming 1µm section thickness there was no significant difference between the estimates of glomerular diameter from either method (t-test; P=0.325) and no correction was needed for section thickness or measurements of length in the sectioning direction (z).

The glomerular diameters ($2r_x$ $2r_y$ $2r_z$) measured during the calibration of section thickness were used to calculate glomerular volume ($V_G = 1.33\ \pi\ r_x\ r_y\ r_z$).

Glomerular and vascular orientation in resin section reconstruction

Vascular pole recognition was most easily achieved in 1µm serial resin sections where the section plane was par-axial with the *vascular pole* - *urinary pole* axis of the glomerulus, as a result reconstructed glomeruli were sectioned close to a paraxial plane. The true diameters of any vessel profile was measured by searching the sequential images for the appropriate vessel section and measuring vessel width (x,y). Section depth diameter was taken from the limits of vessel walls in the sectioning direction (z). Vessel lengths (between branch points for example) through the image stack were measured on section if possible or by triangulating through the stack using sectioning depth and horizontal 'on section' distance.

The three diameters of VCs (x,y and z) used to calculate the means in table 1 and 2 were further used to calculate afferent and efferent vascular chamber volume ($V_{AVC} = 1.33\ \pi\ r'_{AVC}\ r''_{AVC}\ r'''_{AVC}$; $V_{EVC} = 1.33\ \pi\ r'_{EVC}\ r''_{EVC}\ r'''_{EVC}$).

Bends between arterioles and VCs were assessed in resin section image stacks of 10 glomeruli by assessing the afferent and efferent arteriole axis vector and measuring the change in angle into the VC axis vector (Fig.3A). This included measurements on section and in the sectioning direction and triangulation in vessels moving at angles to the section plane.

Afferent first order (conduit) vessel ballooning in resin sections

Any ballooning or hyperinflation of first order afferent (conduit) vessels was estimated initially by comparing conduit diameters in areas of potentially high transmural pressure gradient (conduit vessels with large areas of GFB, 0-60% mesangial cover) with

conduit diameters in areas of potentially low transmural pressure gradient (conduit vessels with 80-100% mesangial cover). These data were further dissected in each conduit vessel by subdividing the initial 0-60% mesangial cover group into 4 groups and using the 80-100% mesangial cover group as a baseline to calculate the fold change in diameter.

Podocyte cell body coverage of conduit vessels

Podocyte cell body (PCB) coverage on the urinary side of conduit vessels was estimated by measuring length of GFB in a vessel image covered by a visible podocyte cytoplasmic region and the accompanying areas where no cell body was apparent. This was compared with similar measurements from filtration capillaries.

VC recognition in single resin sections

To test whether evidence of VCs could be seen in single sections of glomeruli (being the more common way of looking at human biopsy glomeruli) the occurrence of widened vasculature at the vascular poles was assessed in single sections of renal cortex. In an additional 13 resin-embedded human kidneys, immersion and perfusion fixed single cortical sections (1µm thick) were stained with Toluidine Blue. Glomerular sections showing vascular poles were assessed for the frequency of vascular widening around the poles. Width was assessed by placing an ellipse around widened vascular profiles and taking the minimum diameter to eliminate oblique vascular diameter measurements.

Confocal and multiphoton light microscopy on fresh kidney slices

Aqueous fresh and fixed kidney was observed using confocal and multiphoton microscope techniques.

A Nikon confocal microscope (Nikon Eclipse Ti) was set to image fixation induced autofluorescence (FIA). Millimetre and sub millimetre thick fixed renal cortical slices were washed in HEPES Ringer solution and the autofluorescent signal (FIA) at 488nm wavelength was used to image and obtain z stacks from glomerular vascular poles of up to 100µm depth from the cut surface.

Using a multiphoton microscope, two fresh and two fixed unstained slices of renal cortex, were imaged as previously described (2). Two imaging modes were applied, fibrous collagen was visualised using second harmonic generation (SHG) and elastin from its intrinsic two photon fluorescence (TPF) along with any background fluorescence. TPF and SHG images were obtained using a modified confocal microscope (FluoView IX71 and F300, Olympus). Signal was produced using the 800 nm output of a mode-locked Ti:sapphire laser (Mira 900-D, Coherent Inc) pumped by a 532 nm solid state laser (Verdi V10, Coherent Inc.). The pulsed laser had a pulse width of 100 fs and a repetition rate of 76 MHz. The light was focused on to the sample using a 60X 1.2 NA water immersion objective (UPlanS Apo; Olympus). Signal was collected in the epi-direction using the objective lens and separated from the laser fundamental using a long pass dichroic mirror (670dcxr; Chroma Technologies). The signal was then passed through two filters (for TPF: CG-BG-39 and F70-500-3-PFU; and for SHG: CG-BG-39 and F10-400-5-QBL; CVI Laser) before being focused on a photomultiplier tube (R3896, Hamamatsu). Each 1024×1024 pixel image took 29 seconds to acquire, meaning a stack

of 100 images, each separated in the z-direction by 1 μm, took approximately 50 minutes to complete.

Electron microscopy

From 1μm Resin sections of renal cortex showing identifiable VCs, further sections were cut at 70-100nm thickness and stained with 10% Phosphotungstic acid (10 minutes). Sections were viewed and digital images taken on a Tecnai T12 (FEI UK Ltd).

Calculation of vascular resistance

The resistance to flow along the terminal part of the arterioles will change as blood enters AVCs and conduits, and exits EVCs. Assessing such resistances may give a better understanding of how blood flow will be affected by VCs and conduits, **a** correlate of total conduit resistance per unit length (R'_{Con}) was derived from the Poiseuille equation (see Appendix 1)

$$R'_{Con} = \frac{1}{r_{Con}^4 . n_{Con}} \qquad \text{Eq.1}$$

Where r_{Con} is the mean conduit vessel radius and n_{Con} is the number of conduit vessels merging from an AVC. R'_{Con} provides a value that scales proportionately with total vascular resistance per unit length. Similarly a correlate of first order efferent (E1) resistance per unit length (R'_{E1}) was estimated from $1/r_{E1}^4 n_{E1}$ and arteriole resistance per unit length (R'_{AA}, R'_{EA}) was calculated from $1/r_{AA}^4$ and $1/r_{EA}^4$.

Statistics

Data were represented throughout as either mean ± standard error of the mean or as median (interquartile range). Excel was used for collating data and initial statistics, Prism software (Graphpad Software Inc.) was used for statistical analysis generating histograms, correlations, parametric and non-parametric tests.

Results

Glomerular structure from resin serial section image stacks

Glomerular Arterioles

Assigning afferent and efferent labels to arterioles was accomplished by tracing the origin of these vessels in the serial section image stacks. Branches of cortical radial or interlobular arteries (38, 58) were traced to the afferent arterioles (Fig.1) and efferent vessels showed a characteristic peritubular branching course on emerging from glomeruli.

Afferent and efferent arteriole wall thickness were significantly different (6.6±0.3μm, 3.0±0.1μm respectively, paired t-test $p<0.0001$ n=7) as were afferent and efferent luminal diameter (23.2±1.8μm, 17.6±2.0μm respectively, paired t-test $p=0.02$ n=7). Wall thickness being a better predictor of arteriole type than luminal diameter. No correlation was found between the afferent (R'_{AA}) and efferent (R'_{EA}) arteriole resistance measure (Tab.3 $R^2 = 0.033$ $P=0.53$).

The efferent picture was confused by multiple efferent arterioles in 4 out of 14 glomeruli. Major efferent arterioles have been shown in table 2, the extra 1 to 3 minor efferents were in series or parallel with EVC and were 4.6-8µm diameter with one 11.5µm in series with an efferent VC. No extra afferent arterioles were seen.

Reconstruction of VCs and 1st order vessels

All 14 glomeruli (4 kidneys) analysed from image stacks of 1µm resin serial sections showed afferent and efferent widening of the arterioles, resulting in vascular chambers (VCs) embedded in the mesangium of the vascular pole (Fig.2, see supplemental video 2a and 2b for full image stacks). Some afferent VCs (AVCs) protruded into a hilar or juxta-glomerular position (sections 198 & 209, Fig.2B).

Vascular width and connectivity is illustrated in a scale diagram in figure 3A, (measurements from tables 1&2). To summarize, the 21µm diameter afferent arteriole (AA) leads into an ellipsoidal afferent vascular chamber (AVC; 49x48x32µm) which branches into on average 7 first order afferent vessels of 16µm diameter we have termed conduit vessels (Con; Fig.2A, B, Fig.3A, Tab.1). These vessels had secondary vessels (A2) emerging at spacings of 32.8µm (median), with 41% of branches intervals between A2 greater than 40µm with a quarter of these above 100µm (Fig.4A). Conduit branches into A2 were more frequent distal to the AVC at the glomerular edge (Fig.2B. & supplemental video 2a and 2b). Conduit vessels coursed through mesangium and then either through the centre of the glomerulus or peripherally over the glomerular surface before branching into capillary networks (Fig.2A & B) [Supplementary videos S2c and S2d (Fig.2B as a reconstructions)].

At the efferent end of the filtration capillary network first order efferent vessels (E1) were more numerous (13 v. 7) and narrower than conduits (10µm v. 16µm diameter; Fig.4B; Tab.1&2). Secondary efferents (E2) merged at 15µm intervals into 13 first order vessels (E1) (Figs.2A, B & 3A). Only 4% of E2 branch intervals on E1 vessels were above 40µm - (Fig.4A). E1s converged into an efferent vascular chamber (EVC; 46x43x26µm) in turn disgorging into a 16µm diameter efferent arteriole (EA; Figs.2A, B & 3A, Tab.2).

In 10 of the 14 glomeruli where the orientation of afferent and efferent arterioles on entry into the VCs could be easily assessed, the AA bent 60º off its straight track into the AVC (AA/AVC angle = 120±6˚), similarly, the EA bent 71º off track into EVC (EA/EVC angle = 109±7º Fig.3A).

VC and glomerular size

AVC volume (V_{AVC} = 41±5x10^3µm^3) was 1.6 fold greater than EVC volume (V_{EVC} =28±7 x 10^3µm^3), with no correlation between them (R^2 = 0.164 P=0.152). V_{AVC} varied over a greater size range (15-70x10^3 µm^3) with V_{EVC} more conserved (12 out of 14 between 10-40x10^3µm^3). Both V_{AVC} and V_{EVC} correlated significantly with V_G (Fig.4C, D, Tab.4), V_G being 100 fold larger than V_{AVC} and 150 fold larger than V_{EVC} 150. This implies a relationship of both the input the output manifold with the magnitude of the perfused volume.

If the glomerular and VC volume (Fig.4C, D) correlation is extrapolated back from larger glomeruli then a minimal VC volume can be reached where the volume describes a mere continuation of the attached arteriole (Fig.3B). Accordingly, a

cylindrical minimum VC volume was calculated using average VC length (L) and arteriole radius (r), a minimum AVC volume of $1.57x10^4 \mu m^3$ would occur at a V_G of $2.2x10^6 \mu m^3$ (Fig.4c). Similarly, a minimum EVC volume of $0.75x10^4 \mu m^3$ would occur at a V_G of $2.9x10^6$ μm^3(Fig.4D). Translating V_G into glomerular diameter, VCs would be minimal (a continuation of the arteriole) in human glomeruli below 160-180µm diameter (i.e.$V_G = 2 - 3x10^6 \mu m^3$).

Conduit podocytes

In resin section image stacks spanning a conduit vessel, we noted a significant lack of coverage of podocyte cell bodies (PCB) over the GFB surface (e.g.Fig.2A Con in sections 312 & 329; Supplemental 2a & 2b). Narrower, shorter first order efferent vessels (E1) were embedded in mesangium adjacent to the EVC and so had zero podocyte coverage (e.g.Fig.2B E1 in sections 249, 258 & 266). PCB area coverage was estimated in GFB conduit regions (n=10, i.e.Fig.2; GFB.Con Fig.3) and small filtration capillary regions (n=22) from 4 human glomeruli. Conduit vessel PCB area coverage was halved compared with small filtration capillaries (29±3% v. 55±3%; ttest - P<0.0001; Fig.5B).

Conduit mesangial support

Conduit vessels proceed from a central glomerular region with mesangium on all sides (Fig.3A Mes.Con) to regions with less mesangial attachment and areas of filtration barrier (Fig.3A GFB.Con). Appendix 2 shows that moving from mesangial supported regions of conduit to regions where this support is replaced by GFB more than doubles the hoop stress tending to inflate or expand the vessel wall. To test if the GFB conduit regions showed any ballooning due to lack of mesangial support, conduit vessel diameters measured in 13 glomeruli (resin reconstruction method) were the same in high (80-100% mesangial cover) and low mesangial cover regions overall (17.7±0.8µm,17.9±0.4µm respectively, paired t-test, n=61, p=0.28). However, after further division of the low mesangial cover data set, conduit vessels with the lowest mesangial cover (<15% mesangium, >85% GFB) showed significant inflation of 7% compared to high mesangial cover regions close to the AVC (paired t-test P=0.04, Wilcoxon P=0.04; Fig.5A).

Vascular Resistance and volume relationships

Since Poiseuille flow conditions do not apply to an ellipsoidal chamber manifold with many branches, the vascular resistance per unit length could not be calculated for VCs, therefore their capacity, V_{AVC} or V_{EVC}, was compared with glomerular vessel resistance parameters. Glomerular volume (V_G) was used as a correlate of perfusion volume and compared with the resistance parameters.

R'_{AA} did not correlate with any of the other R′ parameters or V values, no correlation was found between R'_{AA} for afferent arterioles and V_{AVC} (R^2 = 0.014, P=0.68) or V_G which it supplies (R^2 = 0.065, P=0.38) (Tab.3). From the afferent VC there was a significant negative correlation between V_{AVC} and R'_{Con} (R^2 = 0.327, P=0.033; Fig.5C; Tab.3) showing that as the input manifold gets larger the supply conduits to the filtration capillary regions get proportionally more conductive (wider).

On the efferent side there was no similar correlation between efferent first order vessels R'_{E1} and V_{EVC} (R^2 = 0.088, P=0.303) though both of these correlated with V_G

implying a link with perfusion volume. No correlation was found between R'_{EA} and V_{EVC} (R^2 = 0.22, P=0.094) but R'_{EA} does correlate inversely with V_G (R^2 = 0.47, P=0.007; Fig.5D, Tab.3) and directly with both first order afferents (R'_{Con}) and efferents (R'_{E1}).

Table 3 summarizes the capacity and resistance parameter correlations in the human glomerulus; strikingly, R'_{AA} remains independent of all glomerular parameters but all other glomerular vascular entities appear fluid dynamically tied together.

VC in single resin sections.

Single sections of immersion and perfusion fixed kidney (n=13) revealed randomly orientated profiles of glomeruli with vascular poles (n=177). There was no significant difference in the occurrence of vascular widening at the vascular poles between immersion and perfusion fixed glomeruli or between juxta medullary (JM) and subcapsular (SC) glomeruli (Fig.6A). Analysis of all glomeruli together where no descrimination was made in glomerular position (JMSC) in 8 immersion fixed tissues revealed vascular widening in 53±5% of vascular pole sections. Overall frequency was 60±4% for vascular widening in single sections of glomerular vascular poles.

The widened vascular regions found at SC vascular poles were 28.5±3µm and 30.7±2.1µm (minimal diameter) after immersion or perfusion fixation respectively and represented randomly oriented sections of presumably both vascular chambers. This lack of collapse shows that VCs appear to remain open even when the vascular pressure is reduced during fixation. The full morphology of JM vascular chambers remains to be investigated with serial sections.

VC imaged by confocal and multiphoton microscopy

Using a combination of fixation induced autofluorescence (FIA), two photon fluorescence (TPF) and second harmonic generation (SHG) modes, AVC could be seen with attached wide conduit vessels and AA in both fixed and fresh kidney slices (Fig.7). EVC was more difficult to observe with narrower blood vessels (E1) emerging from them. Measurements of recognised structures show similar dimensions using these optical sectioning methods and resin section reconstruction methods (Tab.4).

In addition to morphology SHG can detect collagen without the need for fixation or labelling. Coherent emission in SHG mode in unfixed glomeruli revealed a signal consistent with banded collagen which when overlaid with co-registered TPF images was positioned in the AVC walls (Fig.7, Supplemental video S3). The collagen sheath extended throughout the AVC and a short distance along the attached conduit vessel walls. A similar banded collagen signal was also seen in fixed tissues. TPF imaging showed fresh glomeruli with extensive vessel collapse in the filtration networks but VCs appeared resistant to collapse as was found with resin section reconstruction and resin single sections.

VC wall appearance under electron microscopy

No visible sign of collagen fibres could be seen in the 1µm light microscopy resin sections. Electron microscopy sections of AVC showed regions of banded collagen fibres in the surrounding mesangial matrix. The banding was sparse and poorly stained (30±1nm band spacing) and width of the fibres (30±2nm) in this partial sheath was consistent with Collagen I and III (Fig.8a-d). The collagen bundles extended to a depth of

4µm from the VC surface (Fig.8C; Tab.4). The endothelial lining of AVC contained few fenestrations together with cellular distortions and membrane blebs (Fig.8C), unlike the abundant fenestral density of the filtration capillaries.

Discussion

Vascular chambers

Human glomerular microvascular architecture is not as depicted in current texts. The vascular layout developed over the last 170 years since William Bowman (5) is of a single afferent arteriole which branches until filtration capillaries are reached. These filtration capillaries converge to form a single efferent arteriole conveying blood to the peri-tubular vasculature. This classic picture has been built up from biopsies or necropsies of mammalian kidney.

In human glomeruli both arterioles exhibit vascular widenings more frequently associated with low pressure veins (venous sinuses of the brain) or with large arteries (carotid sinus). However, the glomerular VCs are high pressure arteriolar afferent and efferent chambers with multiple openings, the closest definition in physical terms is a plenum manifold (plenum - a chamber containing pressurized fluid to control distribution; manifold - a pipe or chamber branching into several openings).

Plenums and manifolds in industry stabilize, distribute or balance fluid flow through multiple inlets and outlets (i.e. inlet and exhaust manifolds on internal combustion engines). Therefore, our initial hypothesis for glomerular vascular chambers is that they function to balance the pressure and/or flow through the intervening filtration regions without the need for conventional branching within the confined space of the glomerulus. These haemodynamic considerations are not relevant in smaller rodent glomeruli with smaller perfusion volumes relative to arteriolar conductivity (see introduction).

These VC manifolds persist in the glomerulus despite pressure changes, VC walls are resistant to collapse during immersion fixation or when observed fresh at zero pressure. The VC position at the vascular pole allows mesangial structural support and Collagen I/III appears to provide (additional) structural integrity. The physiological significance of this collapse resistance is not yet clear.

Collagen III has been observed in glomeruli of collagen nephropathies (7, 14) with collagen III in mesangium and/or capillary walls. No report could be found of Collagen I or III in mesangium of normal glomeruli and this report is the first to find banded Collagen (I and/or III) in normal glomeruli close to the vascular pole. Banded collagen has previously been found in kidney cortex, where 30nm fibres showed hybrid labelling with Collagen I and III (13), however, the identity of VC wall banded collagen remains to be confirmed by immunohistochemistry.

VCs appear to be ubiquitous in the adult kidney. We confined resin section reconstructions in this study to subcapsular glomeruli to surmount any size difference between subcapsular and juxtaglomerular glomeruli seen in humans and other species

(17, 34, 51, 55, 58) Evenso, the resin single section work shows a surprisingly similar occurrence of vascular widening in 50-60% of vascular pole glomerular profiles (Fig.6), implying that VCs exist in both cortical locations with similar sized VCs in both juxta-medullary and subcapsular glomeruli.

Afferent and efferent arterioles

No previous study has measured the diameter of fully opened human glomerular arterioles perfusion fixed at their operating pressures. Previous human AA diameters vary from 13-16μm (18) to diabetic biopsy diameters of 29μm for AA and 19μm for EA(44). Other than biological variability, this range of arteriolar diameter is likely due to: volume changes in tissue processing, oblique sections of vessel or low pressure fixation producing collapsed profiles (for example; Tab.4 fresh AA - 13.8μm; Fig.1 in ref.(45)). These problems appear minimized with the fixation and resin embedding techniques of this paper.

A correlation between afferent arteriolar diameter and mean glomerular capillary area has previously been seen as consistent with loss of autoregulation (18). Here a correlate of AA resistance per unit length (R'_{AA}) did not scale with any other glomerular parameter measured including R'_{EA} (Tab.3) preserving the independent autoregulatory control of AA. In contrast EA resistance per unit length (R'_{EA}) was inversely correlated with V_G (Fig.5D; Tab.3), and correlating remarkably with R'_{Con} at the afferent end (Tab.3). Unlike AA, EA is linked in fluid dynamic terms with the Glomerulus it drains.

Conduit vessels

The first order afferent vessels or conduits were noted by Bowman in 1842, with 2 to 8 branches which visibly ‘subdivide only once or twice as they advance over the surface of the ball’ (5). The few buried deep inside the glomerulus unseen by Bowman may explains the result of 2 to 11 seen in this current study. We also confirm the luminal width of these first order afferent vessels as being as wide as the efferent arteriole (21).

Conduit vessels show fewer branches than their efferent counterparts but branch frequency increases at the start of perfusion regions often at some point on the glomerular periphery (Fig.2). No previous branch data exists for these vessels however, the interbranch length for all rat glomerular vessels at 26.3±24.9μm(SD) (48) is between the medians, 32.8μm (conduit afferent) and 15μm (efferent) of the skewed distributions found here.

Conduit vessels close to the AVC are embedded in mesangium, those distal to the AVC have a GFB. While detailed conduit ultrastructure remains to be confirmed, no aberrant GFB capillary morphology has been noted in all our studies of normal human glomeruli (data not shown). It appears that conduit GFB is similar to filtration capillary GFB except for the scarcity of podocyte cell bodies on the conduit GFB surface. It remains to be determined if conduit podocytes are just responding to local conditions or are a sub-population of conduit podocytes with the extra-long major processes necessary to cover the GFB area in foot processes.

The GFB is known to remain intact and expand under excess pressure (25, 27) and conduit vessels with a 86-100% GFB - or a sparse 0-14% mesangial attachment around the circumference showed diameter expansion by 7% compared to conduit vessels surrounded by and embedded in mesangium (Fig. 5A) - not enough GFB expansion to

explain podocyte cell body free areas on the conduit vessels but below the damaged 'giant capillary' inflation levels previously reported (25). Conduit inflation might be expected considering the reduced podocyte coverage, thin walls and wide diameter and estimates of wall forces show conduit vessels with a high proportion of GFB and low mesangial attachment are the most susceptible to hoop stress of all glomerular vessels (Appendix 2). This marks conduits as a target in hypertensive disease and hoop stress failure has been observed in rat primary afferents (equivalent to conduits) due to glomerular hypertension (with marking albuminuria and glomerulosclerosis) (26).

The subpodocyte space, identified under podocytes (39) should be present under conduit podocyte cell bodies (awaiting EM confirmation). Incidentally, the light microscopy derived filtration capillary podocyte cell body (PCB) area coverage of 55% of the GFB fits well with the electron microscopy derived subpodocyte space coverage of 60% for filtration capillaries found previously (41, 50) suggesting most of human subpodocyte space is under the podocyte cell body.

Other evidence for vascular chambers and conduits

Reconstructed rat glomeruli do not show vascular chambers (48). We confirmed these findings by reconstructing rat glomeruli with Serial Block Face Scanning Electron Microscopy (data not shown) and also found no evidence of VC.

Mammalian arterioles can widen pathologically (32), for instance, mesangiolysis can remove mesangial support causing glomerular vessel aneurysms (35) but such features would not be as highly conserved in shape or have an organized collagenous support as seen in VC found here. Bowman also noted in the larger horse glomerulus that afferent arterioles dilate on the surface prior to dividing but not in human glomeruli (5) we show here that human glomerular vascular dilations are subsurface and would have been invisible to Bowman. The modern conventional description merely reports that the afferent arteriole branches into the glomerular capillary network (22).

VCs may not be present in all human glomeruli, during development, glomerular capillaries arise from one dilated vessel (11) and neonate vascular widening has been shown prior to the five first order afferent branches (21) although this has been ascribed to a vessel remnant from the developing nephron (11). Interestingly, the glomerular diameter increase in children from 112µm (birth) to 167µm (15years) (34) and VC scaling with V_G shows that VCs may not exist in child glomeruli which are below 160-180µm diameter, providing these glomeruli follow the adult glomerular correlation (Fig. 3B & 4C,D). Conduit vessel resistance (R'_{Con}) also scales with V_G, whether this correlation continues in smaller (child) glomeruli or whether the primary afferents in children even constitute 'conduit' vessels needs evaluation.

Renal biopsies do occasionally show evidence of VCs and conduit vessels in section, a survey of images in biomedical journals reveal light micrographs showing a 15µm conduit vessel and 20µm VC (20), a 30µm diameter VC (52) and VCs at both efferent and afferent ends (44). However, without the context of a serial section stack these micrographs remain as widened vascular profiles.

VCs could be artefacts of processing volume changes, however, glomerular diameters (~200µm) derived here were between immersion fixed (160 - 170µm) (10, 31) and autopsy diameters (260-270µm) (8) and closely match in vivo ultrasound values of

200µm (15, 23), suggesting glomerular volume changes during processing were minimal overall.

Wide profiles at the vascular pole in singles sections can be dismissed as collapsed vessels. Put simply, an afferent arteriole terminus of 21µm diameter with a circumference of 66µm could conceivably collapse to a flattened squashed-circle profile approximately 30µm wide which if sectioned longitudinally would fit exactly with the 28-30µm wide profiles measured, however, 60% of randomly oreinted single sections of vascular poles all showed these wide vascular regions - far too frequent for the collapse argument. Additionally, in this study vessel collapse was seen in filtration capillaries in fresh glomeruli (multiphoton microscope: Supplemental Fig. S3) but with VCs held open. VCs are not collapse artefacts but stiff walled vascular structures.

The Murray relationship

The relationship between branching vessel diameters was derived by Murray on the principle of minimum work for blood flow (36, 37) where the radius cubed of the parent vessel equals the sum of the cubes of the daughter vessel radii. The Murray relationship holds for arteries and venules of rat kidney down to the afferent arterioles and venules leading away from the tubular networks (42), but it is not known if it continues into the glomerulus. The Murray relationship in whole human kidney also remains to be assessed.

A Murray constant (K) was calculated for each set of vessels leading into and away from human glomerular VCs in all 14 glomeruli reconstructed from resin sections:

$$K = r^3 n_V \qquad \text{eq.2}$$

Where n_V is the number of vessels and r is the radius. Using r_{AA} , r_{AVC} , r_{Con} , r_{E1} , r_{EVC}, r_{EA} and appropriate n to calculate K, the Murray relationship breaks at the VCs and the first order vessels (conduit and E1 vessels; Fig.6B), where daughter vessels do not have the same Murray constant as parent vessels.

This is an exception to Murray's Law – a plenum/manifold exception, where flow distribution from a single arteriole provides a high pressure distributive flow into many glomerular lobes in a short distance. An estimate of K values for second order afferent vessels (A2 in 2 glomeruli) showed that K may return to the value predicted by the afferent arteriolar radius after skipping the VC and conduit vessels (Fig.6B). Other Murray's law exceptions occur where a higher surface area is required in the exchange vessels of an organ, for instance alveolar capillary networks (59).

The possible mechanisms producing a set of vessels following Murray's law includes an endothelial transducer triggering remodelling after a shear force threshold was exceeded(46). Altering the threshold could induce the vessel diameter changes seen here. However, the Murray relationship requires laminar flow through vessels and the haemodynamic flow will be complex from an afferent arteriole into an ellipsoidal vascular chamber with several outlets.

VC haemodynamics

If glomerular volume is used as a measure of perfusion capacity, it rises and falls along with the size of the AVC and the EVC (Fig.4 C&D). Larger AVCs feed more

blood to larger glomerular filtration regions and thence to larger EVCs. As the size increases the resistance of the conduit vessels, E1 and EA (not AA) falls to accommodate the flow (vessels get wider in proportion to Poiseuille flow) (Fig.5 C&D). All of the major vessels of the human glomerulus past the afferent arteriole are linked in some way in terms of flow and capacity (Tab.3). How would flow progress from laminar flow in an afferent arteriole through the AVC to the conduit vessels? And similarly from efferent E1 vessels through EVC to the efferent arterioles?

A clue to VC flow characteristics comes from the kinks and bends in AAs. One constant feature of the glomeruli analysed is the bend as the afferent arteriole enters the AVC. These bends can be readily seen in the glomeruli of figures 1, 2A and 2B (supplemental videos 2a and 2b) and showed an average 60º deviation from a straight path. The fluid flow at a bend in a channel is known to induce vortices (49), we hypothesize that the summation of all bends in an afferent arteriole (i.e. see bend from interlobular –AA junction in Fig.1) could induce a single major vortex in the AVC possibly aiding distributive flow centrifugally into conduit vessels.

If such a vortex with its axis in the midline of the AVC adopts the properties of a "rigid-body" or "rotational" vortex, then the pressure at the AVC edge at the conduit vessel openings would depend both on the hydrostatic pressure and the dynamic pressure (set by the angular momentum of the moving fluid – $\frac{1}{2}\rho\omega^{2,}$ where ρ=density; ω = angular velocity). Crucially however the dynamic pressures within this form of vortex are uniform (3).

We speculate that in health the AVC and the complex (vortical) fluid movement within it, may ensure a uniform driving pressure into the conduit vessels – maximising a uniform distribution of flow to each of the glomerular lobules. The loss of this equalising distributary mechanism through microvascular disease, mesangial proliferation occluding the AVC, hyperperfusion or immunological injury, could potentially result in localised hyperfiltration and excess shear stress in some glomerular segments with stasis in others. This has implications for glomerular disease in which only some perfused regions of the glomerulus appear to have sustained sclerotic/fibrotic damage (eg FSGS) while adjacent lobules appear normal.

The structure of the efferent vascular chamber, with many microvessels converging on a chamber, lends itself to the development of an irrotational vortex (plug hole vortex) balancing EVC pressure gradients and promoting balanced removal of blood from the glomerular tuft (3).

Conclusion

We show for the first time in human glomeruli that clearly defined afferent arterioles lead into afferent vascular chambers of ellipsoid shape and structure embedded in the mesangium of the glomerular vascular pole and ensheathed in collagen fibrils. These chambers are plenum manifolds with many emergent relatively unbranched wide blood vessels or conduits conveying blood to the periphery of the glomerulus. Branching frequency increases at the end of the conduits leading to filtration capillary networks which lead back to smaller efferent vascular chambers in the mesangium of the vascular pole and then the efferent arteriole. The conduit vessels are sparsely covered with podocytes, and conduit fluid resistance scales with the size of the afferent vascular chambers. Both vascular chambers scale with glomerular capacity suggesting absence of

vascular chambers in glomeruli below 160µm diameter (the glomeruli of children). Resistance correlates of first order afferent (conduit) and efferent vessels and efferent arterioles (but not afferent arterioles) scale together and inversely with glomerular volume. We propose that all these structures represent a large glomerulus adaptation allowing even haemodynamic flow distribution and pressure balance across the many lobes of a human glomerulus.

Appendix 1.

Vascular resistance

The vascular resistance to flow will change as blood flows along AA into AVCs and conduits and later pools in EVCs before flowing into EA. To better understand how blood flow is affected by the changing morphology a correlate of vascular resistance R'_{Con}) was derived from the Poiseuille equation using vessel radii and vessel number. For VCs the flow will be complex and non-laminar in the spheroidal shape and so the Poiseuille equation could not be used so VC volume was used as a measure of VC capacity.

Resistance changes in arterioles and conduit vessels

For conduit vessel resistance ($\sum R_{Con}$) coming out of the afferent VC where R_{Con3} is the resistance of the 3rd conduit vessel in parallel:

$$\frac{1}{\sum R_{Con}} = \frac{1}{R_{Con1}} + \frac{1}{R_{Con2}} + \frac{1}{R_{Con3}} \quad \dots \quad \frac{1}{R_{Conn}} \qquad \text{eqA1.1}$$

For n_{Con} similar conduit vessel resistances R_{ConX}

$$\frac{1}{\sum R_{Con}} = \frac{n_{Con}}{R_{ConX}} \qquad \text{eqA1.2}$$

For fluid of viscosity η, the resistance to flow through a tube of length L is inversely proportional to the 4^{th} power of the radius (Poiseuille's law), similarly:

$$R_{ConX} = \frac{8\,\eta_{Con}\,L_{Con}}{\pi\, r_{Con}^{4}} \qquad \text{eqA1.3}$$

Where L_{Con} is conduit vessel length and r_{Con} the mean conduit vessel radius. If the viscosity of the blood flowing through VC and attached vessels (η_{Con}) is assumed not to

change (low filtration into mesangium in these vessels) then η_{Con} with π and 8 can be combined into a constant k_{Con}:

$$R_{ConX} = \frac{k_{Con} L_{Con}}{r_{Con}^4} \qquad eqA1.4$$

Combining equation eqA1.2 and eqA1.4:

$$\frac{1}{\sum R_{Con}} = \frac{r_{Con}^4 n_{Con}}{k_{Con} L_{Con}} \qquad eqA1.5$$

Inverting eqA1.5 and dividing by L_{Con} and K_{Con} yields a measure of the total conduit vessel resistance per unit length (R'_{Con}).

$$\frac{\sum R_{Con}}{L_{Con} k_{Con}} = \frac{1}{r_{Con}^4 n_{Con}} = R'_{Con} \qquad eqA1.6$$

$1/r_{Con}^4 n_{Con}$ was used to estimate a correlate of vascular resistance per unit length of all conduit vessels in parallel (R'_{Con}). Similarly, 1st order efferents were assessed using $1/r_{E1}^4 n_{E1}$. (R'_{E1}). Correlates of afferent and efferent arteriole resistance per unit length (R'_{AA}, R'_{EA}) were estimated with $1/r_{AA}^4$ and $1/r_{EA}^4$.

Appendix 2.

Vascular wall stress

The conduit vessel wall morphology appears similar to filtration capillaries however, conduits are much wider. Greater diameter tubes or vessels of the same wall thickness are more susceptible to pressure damage or rupture. How might conduit vessel wall stress compare with other glomerular vessels?

VC and conduit vessel wall stress

The effective wall strength and compliance of systemic capillaries is largely due to basement membrane/basal lamina (40). Assuming that glomerular vascular wall strength is due to the glomerular basement membrane (GBM, 0.3µm and less than 1/10th of vessel radius) then the Laplace equation (60) can be used to derive the hoop stress (S_h) of the vascular wall (the force exerted circumferentially trying to pull the wall apart). For cylindrical conduit vessels:

$$S_{hCon} = \frac{\Delta P_{Con} r_{Con}}{t_{Con}} \qquad eq.A2.1$$

Where ΔP_{Con} is the hydrostatic pressure difference across conduit vessel wall of radius r_{Con}, and effective wall thickness t_{Con}.
The equation for a near spherical VC is half that of an equivalent diameter cylinder:

$$S_{hVC} = \frac{\Delta P_{VC}\, r_{VC}}{2\, t_{VC}} \qquad \text{eq.A2.2}$$

Where ΔP_{VC} is the hydrostatic pressure difference across the VC wall of radius r_{VC} , and effective wall thickness t_{VC} . The effective strength of the arteriolar wall will be a composite of strengths of this thick multilayered structure, however, the arteriole smooth muscle wall thins as it transitions into the VC with only endothelium, basal lamina and collagen sheath surrounded by mesangial matrix.

Parameters used in Calculations

S_{hAVC} for afferent VC (AVC):

r_{AVC} = 22µm [mean of r'_{AVC}, r''_{AVC}, r'''_{AVC}; Tab.1],

t_{AVC} = 0.5-4µm [between the first mesangial lamina thickness ~ 0.5µm (see Fig.8d) and the collagen sheath dispersed over 4µm (Tab.4, Fig.8)]

ΔP_{AVC} = 23mmHg [AVC luminal pressure of 63mmHg (43) minus mesangial pressure - a high proportion of capillary hydrostatic pressure (9) - likely 40mmHg since mesangial cells respond to 40mmHg and above (19, 30).

S_{hAVC} = 8 - 66 kPa (equation A2.2) [≤ 8 kPa if the effective ΔP_{AVC} is lower due to pressure dissipating gradients and effective t_{AVC} thicker due to additional mesangial matrix support (7)]

S_{hMC} for mesangial conduit vessel (MC):

The mesangial backed conduit vessels (Fig.3a, Mes.Con) adjacent to AVCs would share the same mesangial protection and possibly collagen sheath as the AVCs.

r_{MC} = 8µm [Tab.1]

t_{MC} = 0.5µm to 4µm [Tab.4, Fig.8]

ΔP_{MC} = 23mmHg [see above]

S_{hMC} = 6 - 48 kPa (equation A2.1) [≤ 6 kPa, S_{hAVC} caveat as above)

S_{hGC} for glomerular filtration barrier conduit vessel (GC):

The conduit vessels away from the AVC are connected to mesangium only on a small part of their circumference the rest being normal GFB and GBM (Fig.3a, GFB Con)

r_{GC} = 8µm [Tab.1]

t_{GC} = 0.3µm [GBM thickness]

ΔP_{GC} = 38mmHg [luminal P (63mmHg) minus urinary space P (25mmHg)]

S_{hGC} = 133 kPa (equation A2.1)

S_{hFC} for filtration capillaries (FC):

r_{FC} = 3.5µm

t_{FC} = 0.3µm [GBM thickness]

ΔP_{FC} = 38mmHg [luminal P (63mmHg) minus urinary space P (25mmHg)]

S_{hFC} = 58 kPa (equation A2.1)

	Subscript abbreviation	ΔP (mmHg)	r (μm)	t (μm)	S_h (kPa)
Afferent VC	AVC	23	22	0.5-4.0	≤8-66
Mesangial conduit	MC	23	8	0.5-4.0	≤6-48
GFB conduit	GC	38	8	0.3	133 *
Filtration Caps.	FC	38	3.5	0.3	58

Table A1. *Calculated vascular hoop stress S_h. The peak is in the GFB conduit vessels (*).*

S_h is difficult to estimate in the mesangial backed AVC and mesangial conduit vessels but our maximum estimate is less than half the value for the GFB Conduit. S_h falls in the filtration capillaries of the same wall thickness but these are protected by their small radius. At the efferent end the reduced radii and complete mesangial encasement of VC and of the short E1 vessels would result in lower S_h of the equivalent efferent vessels (not shown).

In conclusion, in human glomeruli, GFB conduit walls (GC) mark a peak of hoop stress caused by the relatively thin wall for the large diameter. While the AVC and the early conduit vessel are protected by mesangial backing, any mesangial disruption through immune-mediated damage, cell invasion or proliferation or disruption to the collagen sheath will change S_{hAVC} and S_{hMC} making AVC and mesangial conduit vessels vulnerable to pressure changes.

Acknowledgements

This study was financed by The Richard Bright Research Trust until 2014 and then by Kidney Research UK (2014-2015). Early parts of this study have been presented to the British Microcirculation Society annual meetings 2011, 2012 and 2013, 2014, 2015 and to ASN kidney week 2012. We would like to thank W. Brewer, J. Stewer, P. Gurney, P. Davy, D. Widden, H. Hawke, T. Cobleigh and all for their help.

REFERENCES

1. **Arendshorst WJ and Gottschalk CW.** Glomerular ultrafiltration dynamics: historical perspective. *Am J Physiol* 248: F163-174, 1985.
2. **Arkill KP, Moger J, and Winlove CP.** The structure and mechanical properties of collecting lymphatic vessels: an investigation using multimodal nonlinear microscopy. *J Anat* 216: 547-555, 2010.
3. **Batchelor GK.** *An Introduction to fluid dynamics*: Cambridge University Press, 2000.
4. **Bohle A, Aeikens B, Eenboom A, Fronholt L, Plate WR, Xiao JC, Greschniok A, and Wehrmann M.** Human glomerular structure under normal conditions and in isolated glomerular disease. *Kidney Int Suppl* 67: S186-188, 1998.
5. **Bowman W.** On the structure and use of the malpighian bodies of the kidney, with observations on the circulation through that gland. *Phil Trans R Soc Lond* 132: 57-80, 1842.

6. **Boyer CC.** The vascular pattern of the renal glomerulus as revealed by plastic reconstruction from serial sections. *Anat Rec* 125: 433-441, 1956.
7. **Cohen AH.** Collagen Type III Glomerulopathies. *Advances in chronic kidney disease* 19: 101-106, 2012.
8. **Darmady EM, Offer J, and Woodhouse MA.** The parameters of the ageing kidney. *J Pathol* 109: 195-207, 1973.
9. **Elger M, Sakai T, and Kriz W.** The vascular pole of the renal glomerulus of rat. *Adv Anat Embryol Cell Biol* 139: 1-98, 1998.
10. **Ellis EN, Mauer SM, Sutherland DE, and Steffes MW.** Glomerular capillary morphology in normal humans. *Lab Invest* 60: 231-236, 1989.
11. **Evan AP, Jr., Stoeckel JA, Loemker V, and Baker JT.** Development of the intrarenal vascular system of the puppy kidney. *Anat Rec* 194: 187-199, 1979.
12. **Feng MG and Navar LG.** Afferent arteriolar vasodilator effect of adenosine predominantly involves adenosine A2B receptor activation. *Am J Physiol Renal Physiol* 299: F310-315, 2010.
13. **Fleischmajer R, Jacobs L, 2nd, Perlish JS, Katchen B, Schwartz E, and Timpl R.** Immunochemical analysis of human kidney reticulin. *The American journal of pathology* 140: 1225-1235, 1992.
14. **Gubler MC, Dommergues JP, Foulard M, Bensman A, Leroy JP, Broyer M, and Habib R.** Collagen type III glomerulopathy: a new type of hereditary nephropathy. *Pediatric nephrology* 7: 354-360, 1993.
15. **Hall TJ, Insana MF, Harrison LA, and Cox GG.** Ultrasonic measurement of glomerular diameters in normal adult humans. *Ultrasound Med Biol* 22: 987-997, 1996.
16. **Harrison-Bernard LM, Monjure CJ, and Bivona BJ.** Efferent arterioles exclusively express the subtype 1A angiotensin receptor: functional insights from genetic mouse models. *Am J Physiol Renal Physiol* 290: F1177-1186, 2006.
17. **Herbert SC, Reilly, R.F., Kriz, W.** Structural functional relationships in the kidney. In: *Diseases of the Kidney and Urinary Tract* (7th ed.), edited by Schrier RW. Philadelphia: Lippincott Williams & Wilkins, 2001, p. 3-57.
18. **Hill GS, Heudes D, Jacquot C, Gauthier E, and Bariety J.** Morphometric evidence for impairment of renal autoregulation in advanced essential hypertension. *Kidney Int* 69: 823-831, 2006.
19. **Hishikawa K, Oemar BS, and Nakaki T.** Static pressure regulates connective tissue growth factor expression in human mesangial cells. *The Journal of biological chemistry* 276: 16797-16803, 2001.
20. **John R and Herzenberg AM.** Renal toxicity of therapeutic drugs. *J Clin Pathol* 62: 505-515, 2009.
21. **Johnston WB.** A reconstruction of a glomerulus of the human kidney. *Anatomischer Anzeiger* 16: 260-266, 1899.
22. **Kanwar YS, Venkatachalam, M.A.** Ultrastructure of glomerulus and juxtaglomerular apparatus. In: *Handbook of Physiology*, edited by Windhager EE. New York: Oxford University Press, 1992, p. 3-40.
23. **Kessler LW, Fields SI, and Dunn F.** Acoustic microscopy of mammalian kidney. *J Clin Ultrasound* 2: 317-320, 1974.
24. **Kimura K, Tojo A, Matsuoka H, and Sugimoto T.** Renal arteriolar diameters in spontaneously hypertensive rats. Vascular cast study. *Hypertension* 18: 101-110, 1991.

25. **Kriz W, Hackenthal E, Nobiling R, Sakai T, Elger M, and Hahnel B.** A role for podocytes to counteract capillary wall distension. *Kidney Int* 45: 369-376, 1994.
26. **Kriz W, Hosser H, Hahnel B, Simons JL, and Provoost AP.** Development of vascular pole-associated glomerulosclerosis in the Fawn-hooded rat. *J Am Soc Nephrol* 9: 381-396, 1998.
27. **Kriz W, Mundel P, and Elger M.** The contractile apparatus of podocytes is arranged to counteract GBM expansion. *Contrib Nephrol* 107: 1-9, 1994.
28. **Lai EY, Onozato ML, Solis G, Aslam S, Welch WJ, and Wilcox CS.** Myogenic responses of mouse isolated perfused renal afferent arterioles: effects of salt intake and reduced renal mass. *Hypertension* 55: 983-989, 2010.
29. **Lu Y, Fu Y, Ge Y, Juncos LA, Reckelhoff JF, and Liu R.** The vasodilatory effect of testosterone on renal afferent arterioles. *Gend Med* 9: 103-111, 2012.
30. **Mattana J and Singhal PC.** Applied pressure modulates mesangial cell proliferation and matrix synthesis. *Am J Hypertens* 8: 1112-1120, 1995.
31. **McLachlan MS, Guthrie JC, Anderson CK, and Fulker MJ.** Vascular and glomerular changes in the ageing kidney. *J Pathol* 121: 65-78, 1977.
32. **McMillan DE.** The microcirculation in diabetes. *Microcirc Endothelium Lymphatics* 1: 3-24, 1984.
33. **Min W and Yamanaka N.** Three-dimensional analysis of increased vasculature around the glomerular vascular pole in diabetic nephropathy. *Virchows Arch A Pathol Anat Histopathol* 423: 201-207, 1993.
34. **Moore L, Williams R, and Staples A.** Glomerular dimensions in children under 16 years of age. *J Pathol* 171: 145-150, 1993.
35. **Morita T and Churg J.** Mesangiolysis. *Kidney Int* 24: 1-9, 1983.
36. **Murray CD.** The Physiological Principle of Minimum Work: I. The Vascular System and the Cost of Blood Volume. *Proc Natl Acad Sci U S A* 12: 207-214, 1926.
37. **Murray CD.** The Physiological Principle of Minimum Work: II. Oxygen Exchange in Capillaries. *Proc Natl Acad Sci U S A* 12: 299-304, 1926.
38. **Navar LG, Evan AP, and Rosivall L.** Microcirculation of the kidneys. In: *The Physiology and Pharmacology of the Microcirculation*, edited by Mortillaro NA: Academic press, 1983, p. 397-488.
39. **Neal CR, Crook H, Bell E, Harper SJ, and Bates DO.** Three-dimensional reconstruction of glomeruli by electron microscopy reveals a distinct restrictive urinary subpodocyte space. *J Am Soc Nephrol* 16: 1223-1235, 2005.
40. **Neal CR and Michel CC.** Effects of temperature on the wall strength and compliance of frog mesenteric microvessels. *J Physiol* 526 Pt 3: 613-622, 2000.
41. **Neal CR, Muston PR, Njegovan D, Verrill R, Harper SJ, Deen WM, and Bates DO.** Glomerular filtration into the subpodocyte space is highly restricted under physiological perfusion conditions. *Am J Physiol Renal Physiol* 293: F1787-1798, 2007.
42. **Nordsletten DA, Blackett S, Bentley MD, Ritman EL, and Smith NP.** Structural morphology of renal vasculature. *Am J Physiol Heart Circ Physiol* 291: H296-309, 2006.
43. **Oken DE.** An analysis of glomerular dynamics in rat, dog, and man. *Kidney Int* 22: 136-145, 1982.

44. **Osterby R, Bangstad HJ, and Rudberg S.** Follow-up study of glomerular dimensions and cortical interstitium in microalbuminuric type 1 diabetic patients with or without antihypertensive treatment. *Nephrol Dial Transplant* 15: 1609-1616, 2000.
45. **Osterby R, Hartmann A, and Bangstad HJ.** Structural changes in renal arterioles in Type I diabetic patients. *Diabetologia* 45: 542-549, 2002.
46. **Painter PR, Eden P, and Bengtsson HU.** Pulsatile blood flow, shear force, energy dissipation and Murray's Law. *Theor Biol Med Model* 3: 31, 2006.
47. **Preston K, Jr., Joe B, Siderits R, and Welling J.** Three-dimensional reconstruction of the human renal glomerulus. *J Microsc* 177: 7-17, 1995.
48. **Remuzzi A, Brenner BM, Pata V, Tebaldi G, Mariano R, Belloro A, and Remuzzi G.** Three-dimensional reconstructed glomerular capillary network: blood flow distribution and local filtration. *Am J Physiol* 263: F562-572, 1992.
49. **Rowe M.** Measurements and computations of flow in pipe bends. *J Fluid Mech* 43: 771-783, 1970.
50. **Salmon AH, Toma I, Sipos A, Muston PR, Harper SJ, Bates DO, Neal CR, and Peti-Peterdi J.** Evidence for restriction of fluid and solute movement across the glomerular capillary wall by the subpodocyte space. *Am J Physiol Renal Physiol* 293: F1777-1786, 2007.
51. **Samuel T, Hoy WE, Douglas-Denton R, Hughson MD, and Bertram JF.** Determinants of glomerular volume in different cortical zones of the human kidney. *J Am Soc Nephrol* 16: 3102-3109, 2005.
52. **Sato Y, Hara S, Fujimoto S, Yamada K, Sakamaki H, and Eto T.** Minimal change nephrotic syndrome after allogenic hematopoietic stem cell transplantation. *Intern Med* 43: 512-515, 2004.
53. **Shimizu H, Shinohara N, and Yokoyama T.** Topological analysis of the three-dimensional structure of the human renal glomerulus using a computer-aided reconstruction system. *Microvasc Res* 36: 130-139, 1988.
54. **Skov K, Mulvany MJ, and Korsgaard N.** Morphology of renal afferent arterioles in spontaneously hypertensive rats. *Hypertension* 20: 821-827, 1992.
55. **Sorensen FH.** Quantitative studies of the renal corpuscles. I. Intraglomerular, interglomerular and interfocal variation in the normal kidney. *Acta Pathol Microbiol Scand A* 80: 115-124, 1972.
56. **Stout LC and Whorton EB.** Pathogenesis of extra efferent vessel development in diabetic glomeruli. *Hum Pathol* 38: 1167-1177, 2007.
57. **Troncoso Brindeiro CM, Lane PH, and Carmines PK.** Tempol prevents altered K(+) channel regulation of afferent arteriolar tone in diabetic rat kidney. *Hypertension* 59: 657-664, 2012.
58. **Venkatachalam MA, Kriz, W.** Anatomy. In: *Heptinstall's Pathology of the Kidney* (5th ed.), edited by Jennette JC, Olson, J.L., Schwartz, M.M., Silva, F.G. Philadelphia: Lippincott Raven, 1998, p. 3-66.
59. **West JB.** *Respiratory Physiology - The Essentials*. Baltimore: Williams and Wilkins 1979.
60. **Westerhof N, Stergiopulos, N, Noble, MIM.** *Snapshot on Hemodynamics: An Aid for Clinical Research and Graduate Education*: Springer Verlag, 2010.

61. **Willassen Y and Ofstad J.** Postglomerular vascular hydrostatic and oncotic pressures during acute saline volume expansion in normotensive man. *Scand J Clin Lab Invest* 39: 707-715, 1979.

Figure 1. Afferent arteriole and glomerulus connectivity. Selected light micrographs from a 1µm serial section stack to show the connectivity of an afferent arteriole (25µm diameter) with a small artery (110µm diameter interlobular or feed artery). Identifying the root/route of the vessels entering the glomerulus allows identification of afferent and efferent arterioles. Notice the afferent arteriole goes through a right angle as it enters the glomerulus. AA – afferent arteriole; GC - glomerular capillary; serial section number at bottom right.

Figure 2A&B. Serial resin sections through a glomerulus. Selected light micrographs from 2 complete 1µm serial section series to show the route blood takes from an afferent arteriole (AA) into an afferent vascular chamber (AVC) leading into conduit vessels (Con) of high capacity and few branches. At the other end of the microcirculation many branching efferent 1st order vessels (E1) drain into a smaller efferent vascular chamber (EVC) leading to an efferent arteriole (EA). Serial section numbers at bottom left. Scale bar 100µm in micrograph of section 254 or 198 (see Supplemental video S2A and S2B for glomerular image stacks of Fig.2A and B respectively, Supplemental S2C and S2D for a reconstruction of afferent and efferent parts of Fig.2B)

Figure 3. Scale diagram of glomerular vasculature; the smallest vascular chambers. A/ Scale diagram of the Afferent (light grey) and Efferent (white) ends of the glomerular vasculature. Diagram shows size and branch relationships between arterioles, VCs and 1st order vessels (mesangium close to vascular pole - dark grey) (diameters from tab. 1&2). To illustrate VC volume in relation to attached vessels the length of attached vessels accommodating VC volume has been shown - AVC volume would distribute along 112µm length (delimited by hoops *x, y*) of afferent arteriole (AA) or distribute along 31µm length (delimited by hoops *x', y'*) of 7 conduit vessels (Con; 3 of 7 shown). The EVC volume would fill 138µm length of efferent arteriole (EA; hoops *p, q*) or 28µm length of 13 1st order vessels (E1; hoops *p', q'*, 4 of 13 shown). Scale bar 100µm. A2 and E2 – second order vessel examples. Mes.Con - Conduit vessel embedded in mesangium. GFB.Con - Conduit vessel with GFB surface and minor mesangial attachment. **B/** Minimal Vascular Chambers. The upper diagram shows VC as in our reconstructions but both V_{AVC} and V_{EVC} decrease as V_G decreases (Fig.4c&d). VC shrinkage in the radial direction would reduce the diameter and VC volume until it was a continuation of the attached arteriole (Fig.4 C&D).

Figure 4. Conduit branching and diameter; VC volume scales with glomerular volume. A/ Histogram of branch separation between 2nd order branches (A2 or E2) emerging from 1st order vessels (Con or E1). Branch intervals were assessed in 9 glomeruli, conduit vessels (Con, filled bars) are longer and less branched than 1st order efferent vessels (E1, open bars) (Mann Whitney U test medians (32.8, 15µm), $P<0.0001$). **B/** Histogram of 1st order vessel diameter coming off Vascular Chambers.

Conduit vessels (filled bars) are significantly wider than Efferent first order vessels (open bars), efferent distribution is skewed towards lower values (15.3(12.8-18.9) v. 9.0(7.0-11.1); median(IQR); Mann Whitney U test, $p<0.0001$). **C/** Afferent VC volume and **D/** Efferent VC volume scale with glomerular volume to a highly significant level (R^2 = 0.517 P=0.004; R^2 = 0.419 P=0.012 respectively). A minimum possible V_{AVC} and V_{EVC} (See Fig.3B) is also plotted to show V_G where VCs are a continuation of the attached arteriole (i.e. no VC widening).

Figure 5. Conduit diameter changes with mesangium; conduit podocyte attachment; resistance v capacity examples A/ Conduit diameter changes relative to mesangial cover. Conduit vessel diameters adjacent to the afferent VC with mesangial cover of 80-100% (GFB coverage 0-20%) were compared with diameters of low mesangial covered (distal) regions of the same vessel. The fold change in diameter shows a significant diameter increase of 7.4% (*) when mesangial cover is minimal (0-14% i.e. GFB 86-100%). Paired t-tests and Wilcoxon matched pair test (P=0.04). **B/** Histogram of podocyte cell body (PCB) area coverage of the filtration barrier of conduit vessels (filled bars) and small filtration capillaries (open bars). Conduits have significantly less PCB coverage of the GFB than filtration capillaries (ttest - $P<0.0001$). **C/** Conduit resistance versus Afferent VC volume. A significant negative correlation exists between a correlate of conduit resistance (R'_{Con}) and afferent VC volume (V_{AVC}) (R^2 = 0.327, P=0.033). **D/** Efferent arteriole resistance per unit length (R'_{EA}) reduces in line with increasing V_G (R^2 = 0.47, P=0.007).

Figure 6. Vascular widenings in single sections. Murray constant from vascular radii A/ Observed occurrence of glomerular vascular widening in single sections. The frequency with which widening (implying VC presence) was observed at vascular poles in immersion and perfusion fixed glomeruli. SC - subcapsular glomeruli; JM - juxta-medullary glomeruli; JMSC - JM and SC glomeruli combined. (n = number of kidneys)
B/ In 14 glomeruli a Murray constant ($K = r^3 n_V$; where r is radius, n_V is vessel number; see text) was calculated for the afferent and efferent arteriolar tree leading through the VCs and thence into the 1st order vessels (Con and E1). In 2 glomeruli K was calculated for 2nd order vessels. The Murray relationship of equal K at each vessel level is absent in the AVC, EVC and conduit vessels.

Figure 7. Multiphoton imaging of glomeruli. Images obtained by combining two photon fluorescence (TPF) signal images with second harmonic generation (SHG) images of an unfixed human glomerulus. The capillary walls emit a TPF signal (green) with most of the smaller filtration capillaries showing collapse. A banded Collagen signal (SHG blue) is located adjacent to a VC wall (intense Bowman's capsule Collagen has been blanked). Section s1 is close to the tissues physical surface; A - arteriole, (optical section 1µm deep). S31 shows a wide incomplete region of banded collagen around an uncollapsed region (VC) connected with A in s1. The banded collagen region has disappeared in s37 but offshoots in attached vessels appear in s37 (right of VC) and s52 (left of VC position). Diameter of field - 200µm. (See supplemental video S3 for full section series)

Figure 8. Transmission electron micrographs of Vascular chamber walls. Vascular Chamber were imaged using a Tecnai 12 electron microscope, low power **(A)** shows a vascular pole an AVC, conduit vessels (Con) and urinary space (US). **(B)** Montage of micrographs to show the disposition of the banded collagen fibres around the VC walls. White dotted lines show the extent of the mesangial matrix where banded collagen fibres were evident. **(C)** Area C from montage B with matrix rich in banded collagen (BCM) and where collagen is absent (M). **(D)** Area D from montage B with banded collagen fibres.

Table 1 & 2. Afferent and efferent vascular diameters. Diameters of afferent and efferent vessels from resin embedded glomeruli (14) from 4 human kidneys. In all cases the afferent and efferent arterioles widen to form ellipsoidal chambers with between 2 and 11 high capacity conduit vessels emerging and conveying fluid away to the filtration capillaries. Blood from the filtration capillaries converges into 3 to 22 narrow efferent first order vessels which converge into the Efferent VC and thence the efferent arteriole. [In the 14 glomeruli analysed, 2 extra wide conduit vessels (19-24µm) were found, 1 extrawide E1 drainage vessel (20-27µm) but the branching was frequent as in other E1 vessels]. Vascular chamber dimensions: min.diam.; minimum diameter measured in the section plane avoiding oblique vessel sections. max.diam.; maximum diameter measured in the section plane avoiding oblique vessel sections. Secn. depth diam; diameter measured in the sectioning direction. sem; standard error of the mean

Table 3. Vascular resistance and capacity relationships. Significant correlationships (8 out of 21) between 7 variables measured in human glomerular initial vasculature. Correlates of vascular resistance for afferent arterioles (R_{AA}), Conduit vessels (R_{Con}), first order efferent vessels (R_{E1}) and efferent arterioles (R_{EA}) were compared with each other and with AVC volume (V_{AVC}) glomerular volume (V_G) and EVC volume (V_{EVC}). + positive correlation, – negative correlation; * = $P < 0.05$, ** = $P \leq 0.01$; **** = $P \leq 0.0001$; § higher significance with outlier removed.

Table.4. Vascular diameters and wall thicknesses - all experiments. Comparison of AA, AVC, Conduit, E1, EVC, and EA measurements from resin section reconstruction with the same features in fixed and fresh glomeruli reconstructed from confocal and multiphoton microscope z stacks (SHG and TPF). EVC and AVC values have been averaged together for all 3 axes. AVC Collagen sheath (AVC Coll) enshrouded AVC and some parts of conduit vessels but scant evidence in EVC or E1 (multiphoton microscopy only). G and K indicate numbers of glomeruli and kidneys used. * not all quantities were observable and measureable.

Supplemental

Supplemental video legends

Video S2a. Image stack for Fig 2a glomerulus.

Video to show the full image stack formed by Image J software from original 1µm serial section images. Stills in Fig.2a. Field of view 170 x 200µm approximately.

Video S2b, Image stack for Fig 2b glomerulus.
Video to show the full image stack formed by Image J software from original 1µm serial section images. Stills in Fig.2b. Field of view 190 x 220µm approximately.

Video S2c. Reconstruction x derived from Fig. S2b.
Red afferent arteriole derived vessels meeting with blue efferent arteriole derived vessels at purple points. Rotation around x axis. Not all vessels shown. Scale marks in µm.

Video S2d. Reconstruction y derived from Fig. S2b.
Red afferent arteriole derived vessels meeting with blue efferent arteriole derived vessels at purple points. Rotation around y axis. Not all vessels shown. Scale marks in µm.

Video S3. Reconstruction of an unfixed glomerulus from multiphoton microscope images. TPF and SHG modes were used to image the vessel walls (green) and banded collagen (blue) respectively. The intense blue signal from the collagen of Bowman's capsule was covered by a circular black mask. The afferent arteriole opens into a VC at the 7 o'clock position, the banded collagen signal follows the walls of the VC and into the conduit vessels. Field width 200µm

Footnote 1

[Afferent arteriole conductance estimated from the 4^{th} power of vessel radii (mice, r = 5-6.5µm,(16, 28, 29); rats, r = 7-9.5µm(12, 24, 54, 57); human, r = 11µm[this article]) with human glomerular volume estimated from glomerular diameter (mouse=70µm, rat=120µm and human=200µm)]

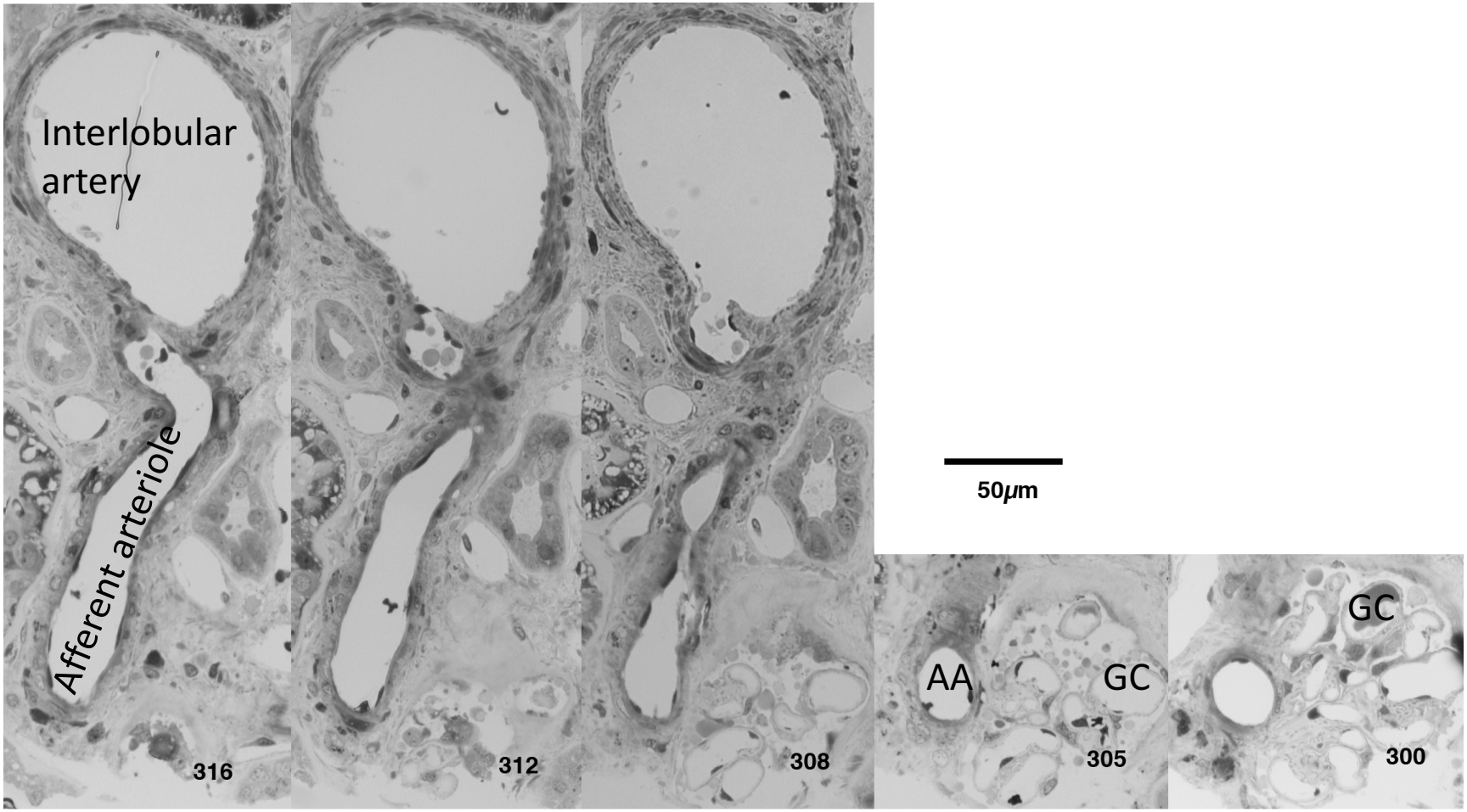

Figure 1. Afferent arteriole and glomerulus connectivity. Selected light micrographs from a 1µm serial section stack to show the connectivity of an afferent arteriole (25µm diameter) with a small artery (110µm diameter interlobular or feed artery). Identifying the root/route of the vessels entering the glomerulus allows identification of afferent and efferent arterioles. Notice the afferent arteriole goes through a right angle as it enters the glomerulus. AA – afferent arteriole; GC - glomerular capillary; serial section number at bottom right.

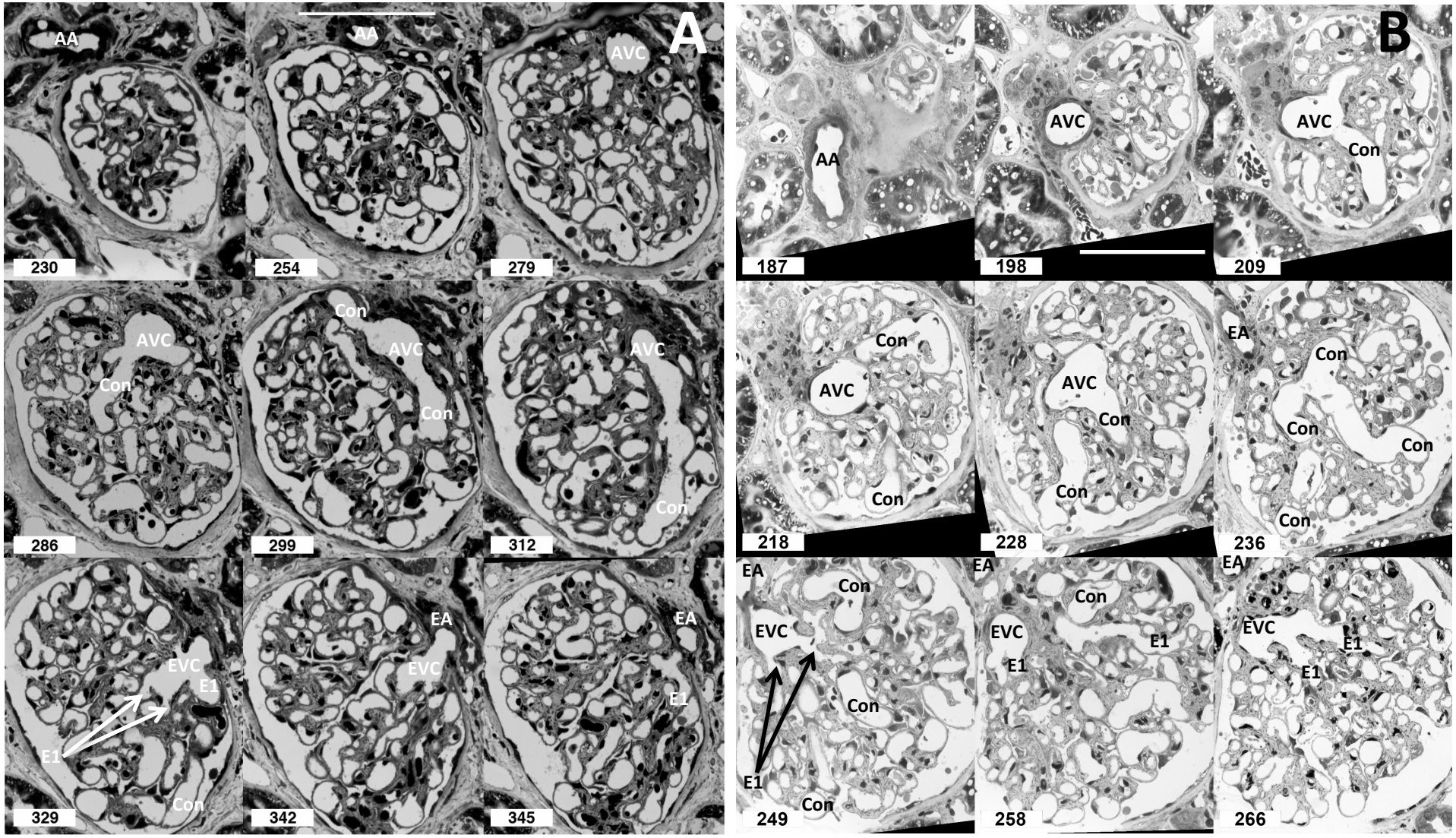

Figure 2A&B. Serial resin sections through a glomerulus. Selected light micrographs from 2 complete 1µm serial section series to show the route blood takes from an afferent arteriole (AA) into an afferent vascular chamber (AVC) leading into conduit vessels (Con) of high capacity and few branches. At the other end of the microcirculation many branching efferent 1st order vessels (E1) drain into a smaller efferent vascular chamber (EVC) leading to an efferent arteriole (EA). Serial section numbers at bottom left. Scale bar 100µm in micrograph of section 254 or 198 (see Supplemental video S2A and S2B for glomerular image stacks of Fig.2A and B respectively, Supplemental S2C and S2D for a reconstruction of afferent and efferent parts of Fig.2B)

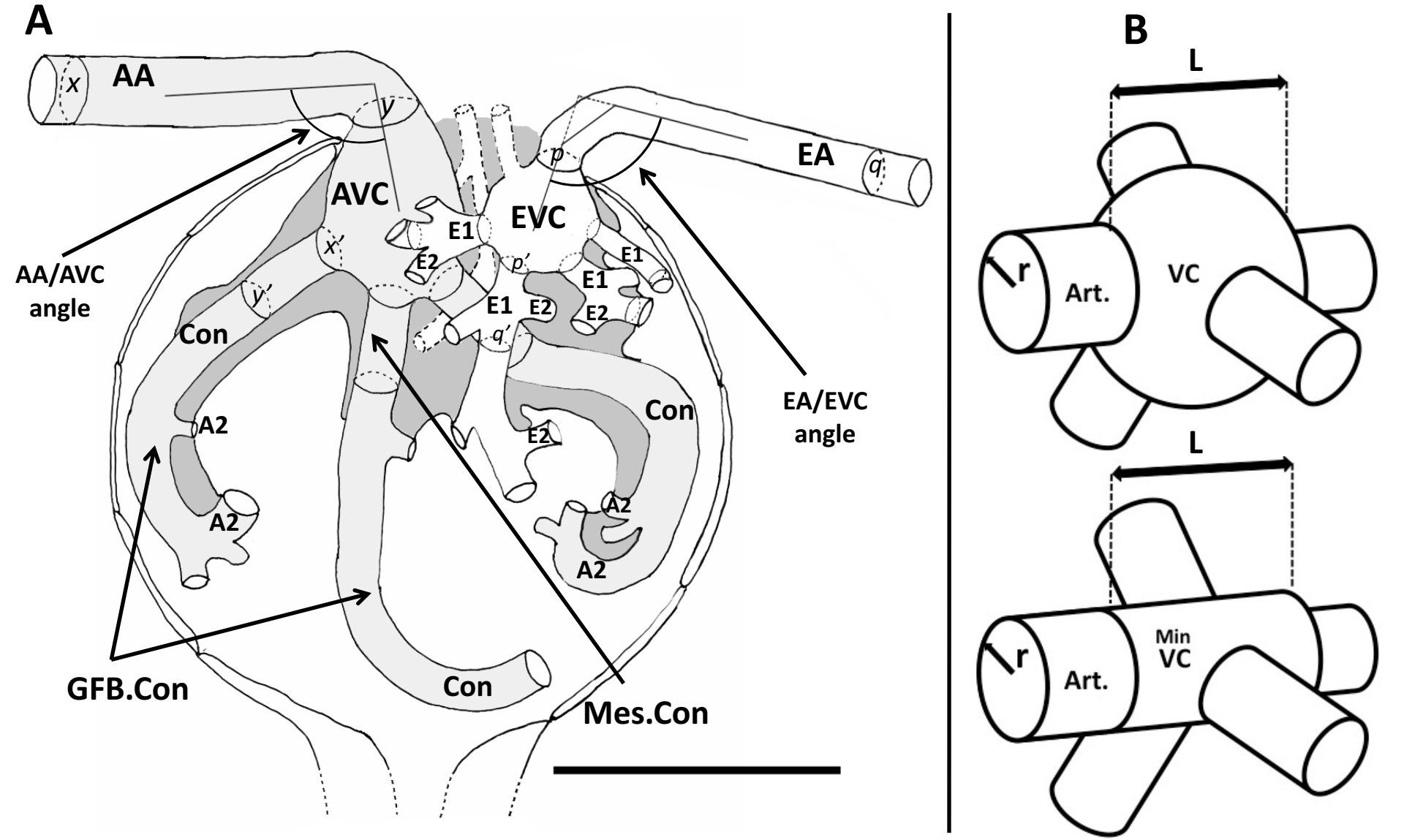

Figure 3. Scale diagram of glomerular vasculature; the smallest vascular chambers. A/ Scale diagram of the Afferent (light grey) and Efferent (white) ends of the glomerular vasculature. Diagram shows size and branch relationships between arterioles, VCs and 1st order vessels (mesangium close to vascular pole - dark grey) (diameters from tab. 1&2). To illustrate VC volume in relation to attached vessels the length of attached vessels accommodating VC volume has been shown - AVC volume would distribute along 112µm length (delimited by hoops *x, y*) of afferent arteriole (AA) or distribute along 31µm length (delimited by hoops *x′, y′*) of 7 conduit vessels (Con; 3 of 7 shown). The EVC volume would fill 138µm length of efferent arteriole (EA; hoops *p, q*) or 28µm length of 13 1st order vessels (E1; hoops *p′, q′*, 4 of 13 shown). Scale bar 100µm. A2 and E2 – second order vessel examples. Mes.Con - Conduit vessel embedded in mesangium. GFB.Con - Conduit vessel with GFB surface and minor mesangial attachment. **B/** Minimal Vascular Chambers. The upper diagram shows VC as in our reconstructions but both V_{AVC} and V_{EVC} decrease as V_G decreases (Fig.4c&d). VC shrinkage in the radial direction would reduce the diameter and VC volume until it was a continuation of the attached arteriole (Fig.4 C&D).

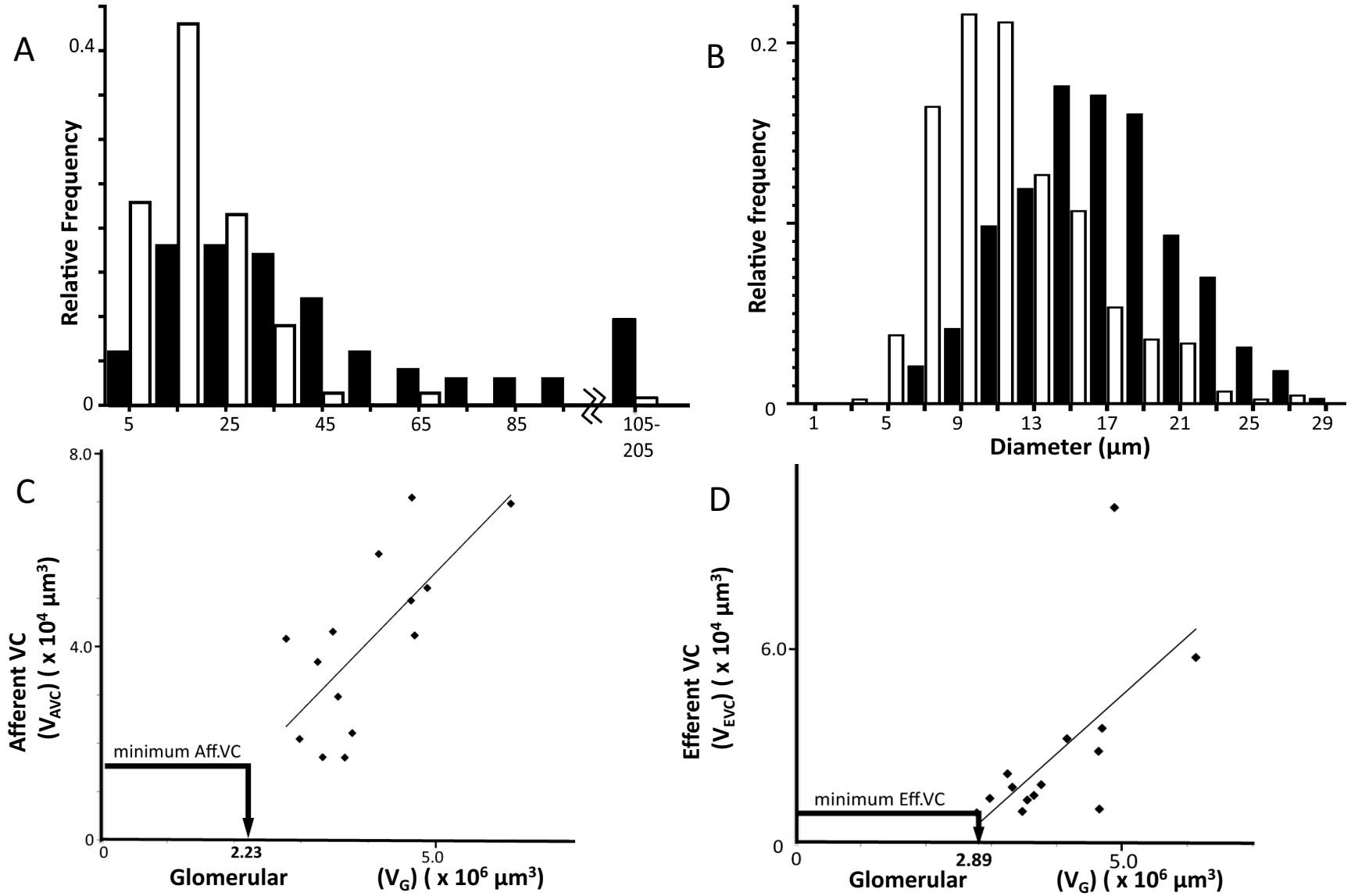

Figure 4. Conduit branching and diameter; VC volume scales with glomerular volume. A/ Histogram of branch separation between 2nd order branches (A2 or E2) emerging from 1st order vessels (Con or E1). Branch intervals were assessed in 9 glomeruli, conduit vessels (Con, filled bars) are longer and less branched than 1st order efferent vessels (E1, open bars) (Mann Whitney U test medians (32.8, 15µm), P<0.0001). **B/** Histogram of 1st order vessel diameter coming off Vascular Chambers. Conduit vessels (filled bars) are significantly wider than Efferent first order vessels (open bars), efferent distribution is skewed towards lower values (15.3(12.8-18.9) v. 9.0(7.0-11.1); median(IQR); Mann Whitney U test, p<0.0001). **C/** Afferent VC volume and **D/** Efferent VC volume scale with glomerular volume to a highly significant level (R^2 = 0.517 P=0.004; R^2 = 0.419 P=0.012 respectively). A minimum possible V_{AVC} and V_{EVC} (See Fig.3B) is also plotted to show V_G where VCs are a continuation of the attached arteriole (i.e. no VC widening).

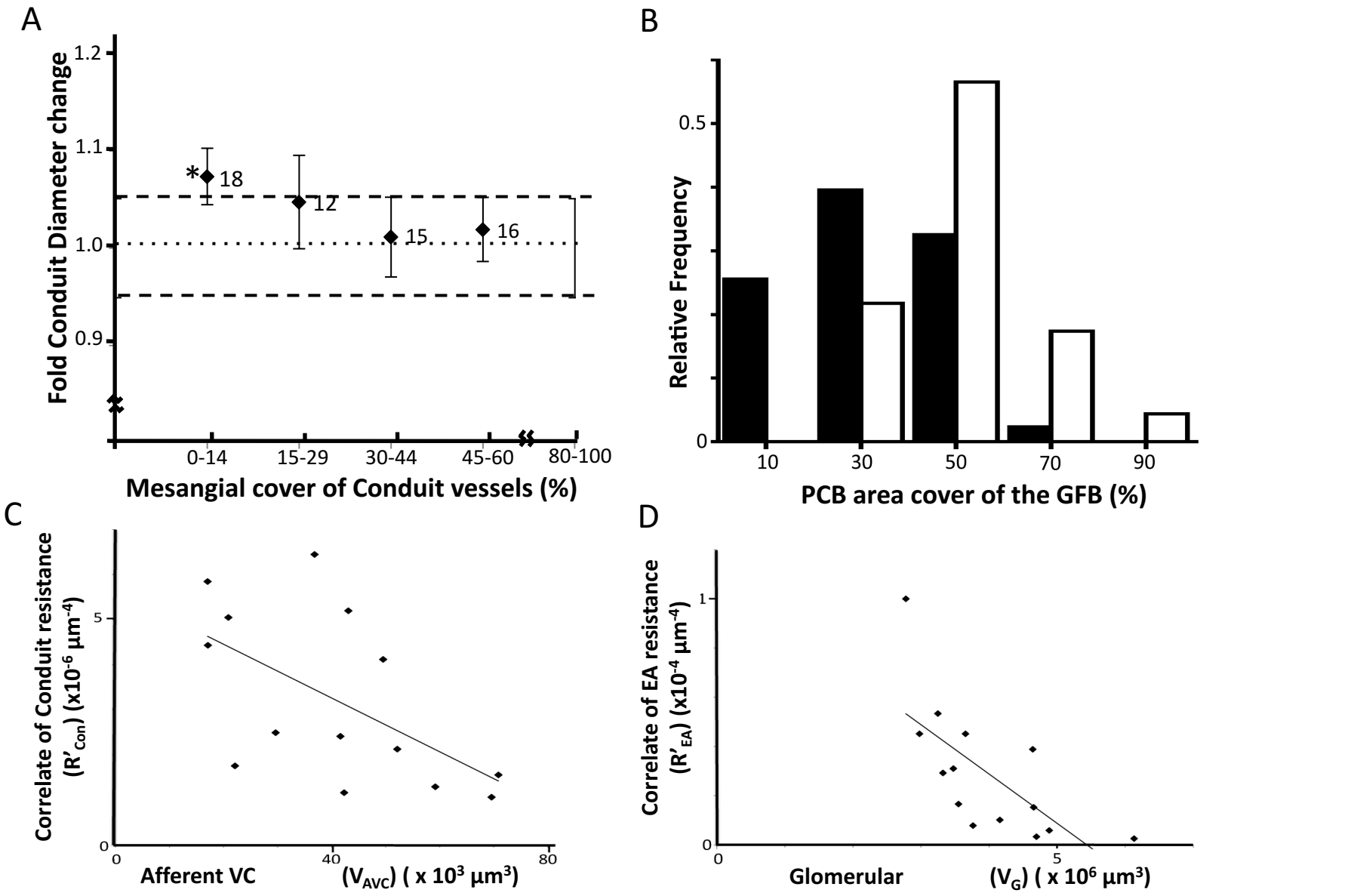

Figure 5. Conduit diameter changes with mesangium; conduit podocyte attachment; resistance v capacity examples **A/** Conduit diameter changes relative to mesangial cover. Conduit vessel diameters adjacent to the afferent VC with mesangial cover of 80-100% (GFB coverage 0-20%) were compared with diameters of low mesangial covered (distal) regions of the same vessel. The fold change in diameter shows a significant diameter increase of 7.4% (*) when mesangial cover is minimal (0-14% i.e. GFB 86-100%). Paired t-tests and Wilcoxon matched pair test (P=0.04). **B/** Histogram of podocyte cell body (PCB) area coverage of the filtration barrier of conduit vessels (filled bars) and small filtration capillaries (open bars). Conduits have significantly less PCB coverage of the GFB than filtration capillaries (ttest - P<0.0001). **C/** Conduit resistance versus Afferent VC volume. A significant negative correlation exists between a correlate of conduit resistance (R'_{Con}) and afferent VC volume (V_{AVC}) (R^2 = 0.327, P=0.033). **D/** Efferent arteriole resistance per unit length (R'_{EA}) reduces in line with increasing V_G (R^2 = 0.47, P=0.007).

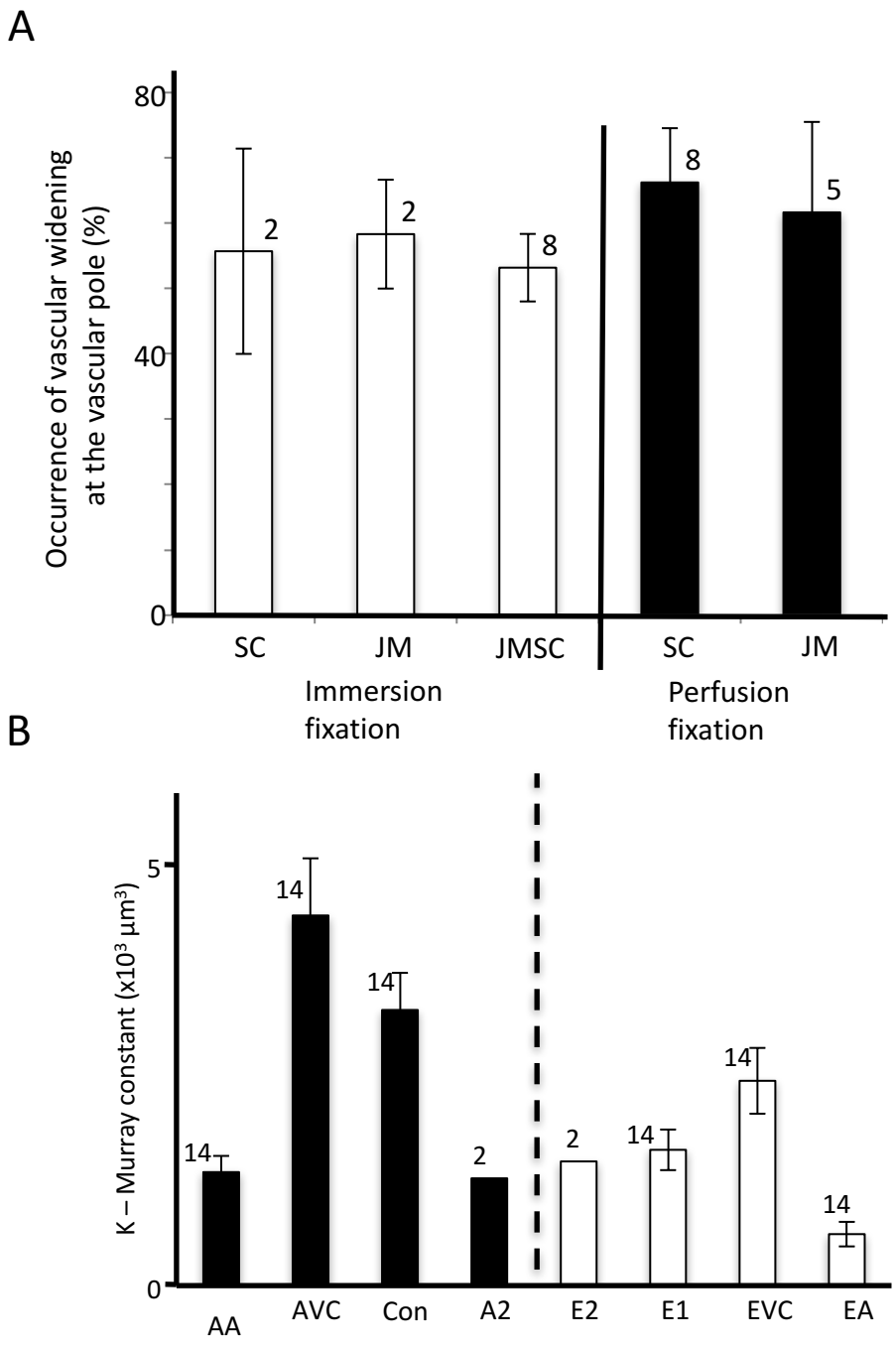

Figure 6. Vascular widenings in single sections. Murray constant from vascular radii A/ Observed occurrence of glomerular vascular widening in single sections. The frequency with which widening (implying VC presence) was observed at vascular poles in immersion and perfusion fixed glomeruli. SC - subcapsular glomeruli; JM - juxta-medullary glomeruli; JMSC - JM and SC glomeruli combined. (n = number of kidneys)

B/ In 14 glomeruli a Murray constant ($K = r^3 n_V$; where r is radius, n_V is vessel number; see text) was calculated for the afferent and efferent arteriolar tree leading through the VCs and thence into the 1st order vessels (Con and E1). In 2 glomeruli K was calculated for 2nd order vessels. The Murray relationship of equal K at each vessel level is absent in the AVC, EVC and conduit vessels.

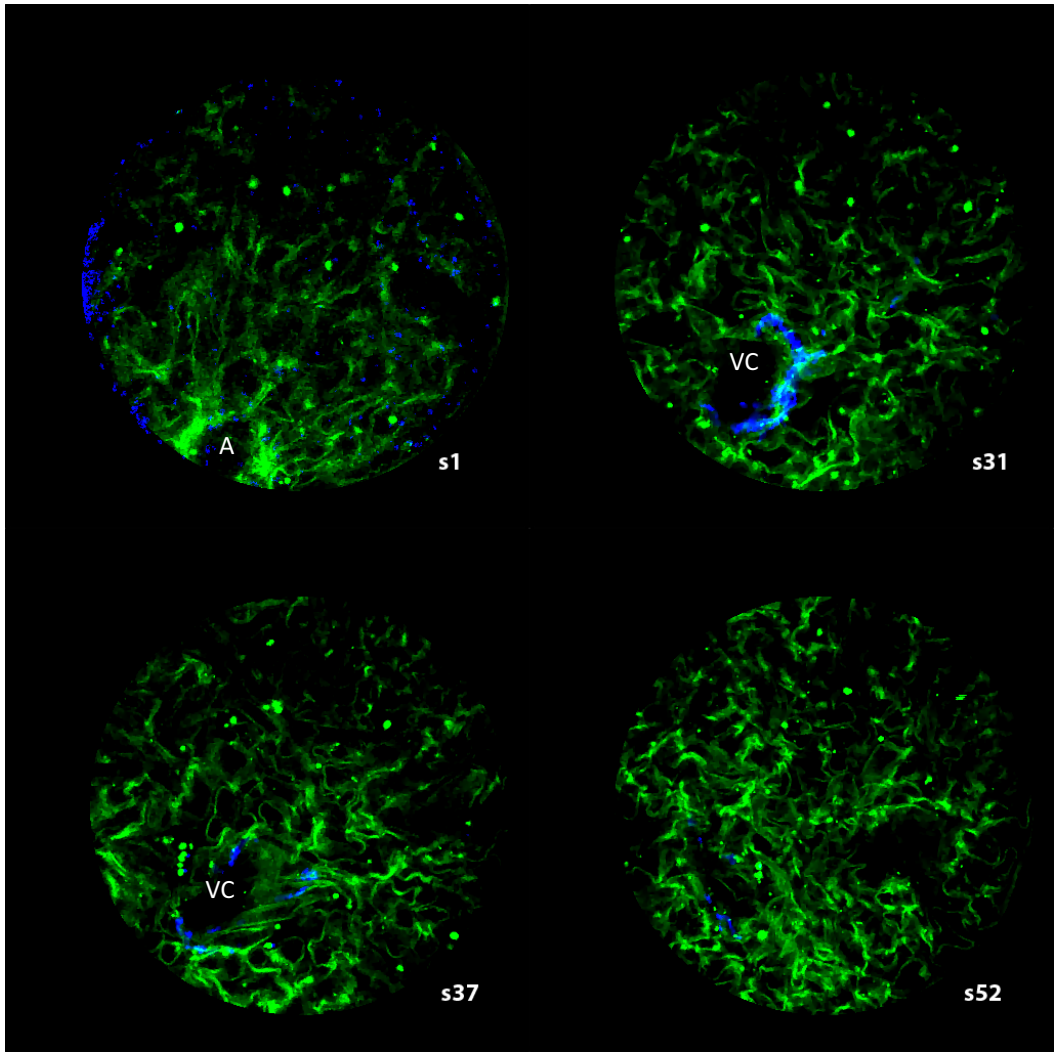

Figure 7. Multiphoton imaging of glomeruli. Images obtained by combining two photon fluorescence (TPF) signal images with second harmonic generation (SHG) images of an unfixed human glomerulus. The capillary walls emit a TPF signal (green) with most of the smaller filtration capillaries showing collapse. A banded Collagen signal (SHG blue) is located adjacent to a VC wall (intense Bowman's capsule Collagen has been blanked). Section s1 is close to the tissues physical surface; A - arteriole, (optical section 1µm deep). S31 shows a wide incomplete region of banded collagen around an uncollapsed region (VC) connected with A in s1. The banded collagen region has disappeared in s37 but offshoots in attached vessels appear in s37 (right of VC) and s52 (left of VC position). Diameter of field - 200µm. (See supplemental video S3 for full section series)

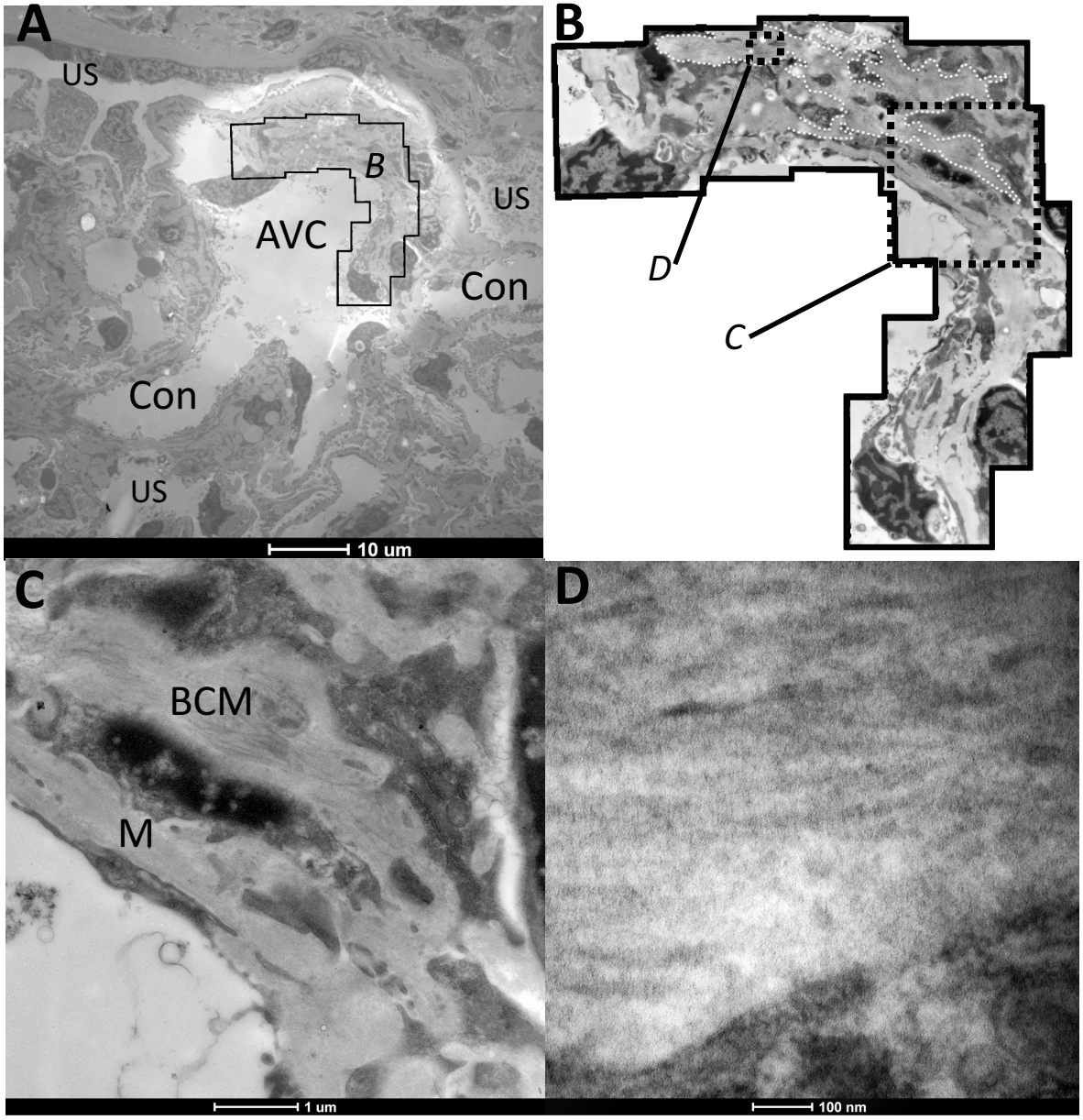

Figure 8. Transmission electron micrographs of Vascular chamber walls. Vascular Chamber were imaged using a Tecnai 12 electron microscope, low power **(A)** shows a vascular pole an AVC, conduit vessels (Con) and urinary space (US). **(B)** Montage of micrographs to show the disposition of the banded collagen fibres around the VC walls. White dotted lines show the extent of the mesangial matrix where banded collagen fibres were evident. **(C)** Area C from montage B with matrix rich in banded collagen (BCM) and where collagen is absent (M). **(D)** Area D from montage B with banded collagen fibres.

Table 1.	**Afferent Arteriole AA**	**Afferent Vascular Chamber AVC**			**Afferent first order vessels Conduit vessels**	
	diameter ($2 r_{AA}$) µm	**min. diam. ($2 r'_{AVC}$)** µm	**Secn.depth diam. ($2 r''_{AVC}$)** µm	**max. diam. ($2 r'''_{AVC}$)** µm	**diameter ($2 r_{Con}$)** µm	**n_{Con}**
mean	**21.5**	**32.1**	**49.4**	**48.0**	**15.9**	**6.6**
sem	**1.2**	**1.5**	**3.4**	**3.6**	**0.7**	**0.6**

Table 2.	**Efferent Arteriole EA**	**Efferent Vascular Chamber EVC**			**Efferent first order vessels E1**	
	diameter ($2 r_{EA}$) µm	**min. diam. ($2 r'_{EVC}$)** µm	**Secn.depth diam. ($2 r''_{EVC}$)** µm	**max. diam. ($2 r'''_{EVC}$)** µm	**diameter ($2 r_{E1}$)** µm	**n_{E1}**
mean	**15.9**	**26.2**	**45.9**	**43.1**	**9.9**	**12.6**
sem	**1.2**	**1.4**	**9.1**	**4.3**	**0.4**	**1.4**

Table 1 & 2. Afferent and efferent vascular diameters. Diameters of afferent and efferent vessels from resin embedded glomeruli (14) from 4 human kidneys. In all cases the afferent and efferent arterioles widen to form ellipsoidal chambers with between 2 and 11 high capacity conduit vessels emerging and conveying fluid away to the filtration capillaries. Blood from the filtration capillaries converges into 3 to 22 narrow efferent first order vessels which converge into the Efferent VC and thence the efferent arteriole. [In the 14 glomeruli analysed, 2 extra wide conduit vessels (19-24µm) were found, 1 extrawide E1 drainage vessel (20-27µm) but the branching was frequent as in other E1 vessels]. Vascular chamber dimensions: min.diam.; minimum diameter measured in the section plane avoiding oblique vessel sections. max.diam.; maximum diameter measured in the section plane avoiding oblique vessel sections. Secn. depth diam; diameter measured in the sectioning direction. sem; standard error of the mean

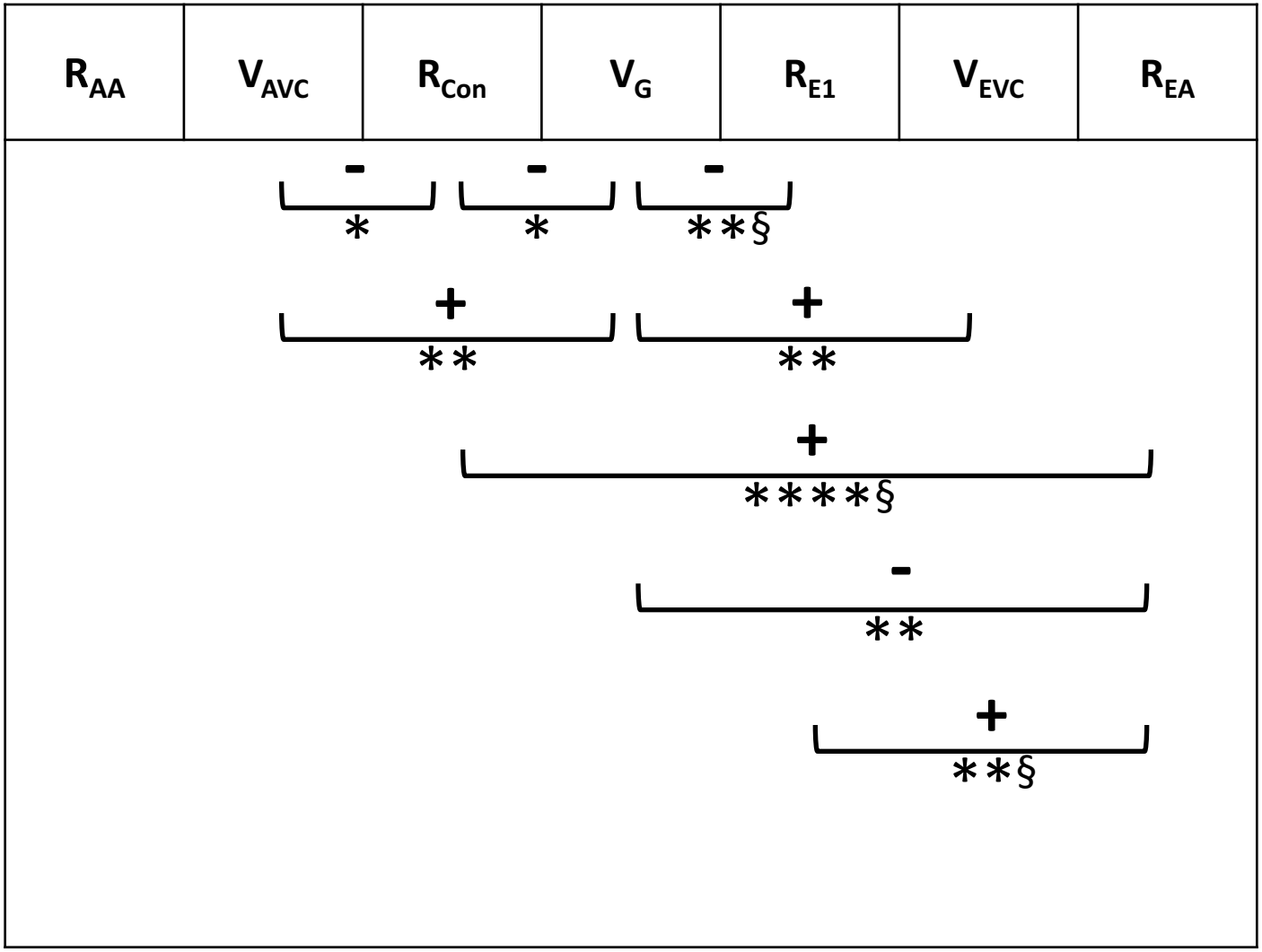

Table 3. Vascular resistance and capacity relationships. Significant correlationships (8 out of 21) between 7 variables measured in human glomerular initial vasculature. Correlates of vascular resistance for afferent arterioles (R_{AA}), Conduit vessels (R_{Con}), first order efferent vessels (R_{E1}) and efferent arterioles (R_{EA}) were compared with each other and with AVC volume (V_{AVC}) glomerular volume (V_G) and EVC volume (V_{EVC}). + positive correlation, − negative correlation; * = $P < 0.05$, ** = $P \leq 0.01$; **** = $P \leq 0.0001$; § higher significance with outlier removed.

		AA	AA	AVC	AVC Coll.	Conduit	E1	EVC	EA	EA
		Diam. (µm)	Wall t (µm)	Diam. (µm)	Wall t (µm)	Diam. (µm)	Diam. (µm)	Diam. (µm)	Diam. (µm)	Wall. t (µm)
Fixed Resin Recon.	14G, 4K	21.5±1.2	6.6±0.3	43.2±2.8	*	15.9±0.7	9.9±0.4	38.4±4.9	15.9±1.2	3.0±0.1
Fixed Aq. Confocal	4G*, 1K	28.4±1.9	6.3±0.8	35.8±3.5	*	16.0±1.2	8.2	24.2	12.8	*
Fixed Aq. Multipho	3G*, 1K	*	*	50.2±3.7	4.2±0.8	12.8±1.6	6.9	28.1	7.4	*
Fresh Aq. Multipho	3G*, 2K	13.8	3.0	35.8±4.1	4.1±1.9	14.4±0.9	*	*	*	*
Fresh Aq. Multipho	Isolated1 G*, 1K	23.0	*	54.2	2.5	27.4	*	*	*	*

Table.4. Vascular diameters and wall thicknesses - all experiments. Comparison of AA, AVC, Conduit, E1, EVC, and EA measurements from resin section reconstruction with the same features in fixed and fresh glomeruli reconstructed from confocal and multiphoton microscope z stacks (SHG and TPF). EVC and AVC values have been averaged together for all 3 axes. AVC Collagen sheath (AVC Coll) enshrouded AVC and some parts of conduit vessels but scant evidence in EVC or E1 (multiphoton microscopy only). G and K indicate numbers of glomeruli and kidneys used. * not all quantities were observable and measureable.